The Journal of Chemical Physics

Single-molecule stretching experiments of flexible (wormlike) chain molecules in different ensembles: Theory and a potential application of finite chain length effects to nick-counting in DNA

Cite as: J. Chem. Phys. **154**, 024903 (2021); https://doi.org/10.1063/5.0028777
Submitted: 08 September 2020 . Accepted: 18 December 2020 . Published Online: 08 January 2021

Ralf Everaers, Nils B. Becker, and Angelo Rosa

The Journal of Chemical Physics ARTICLE scitation.org/journal/jcp

Single-molecule stretching experiments of flexible (wormlike) chain molecules in different ensembles: Theory and a potential application of finite chain length effects to nick-counting in DNA

Cite as: J. Chem. Phys. 154, 024903 (2021); doi: 10.1063/5.0028777
Submitted: 8 September 2020 • Accepted: 18 December 2020 •
Published Online: 8 January 2021

Ralf Everaers,[1,a] Nils B. Becker,[2,b] and Angelo Rosa[3,c]

AFFILIATIONS

[1] Université Lyon, ENS de Lyon, CNRS, Laboratoire de Physique and Centre Blaise Pascal, F-69342 Lyon, France
[2] German Cancer Research Center, Neuenheimer Feld 580, D-69120 Heidelberg, Germany
[3] Scuola Internazionale Superiore di Studi Avanzati (SISSA), Via Bonomea 265, 34136 Trieste, Italy

[a] ralf.everaers@ens-lyon.fr
[b] nils.becker@dkfz.de
[c] **Author to whom correspondence should be addressed:** anrosa@sissa.it

ABSTRACT

We propose a formalism for deriving force–elongation and elongation–force relations for flexible chain molecules from analytical expressions for their radial distribution function, which provides insight into the factors controlling the asymptotic behavior and finite chain length corrections. In particular, we apply this formalism to our previously developed interpolation formula for the wormlike chain end-to-end distance distribution. The resulting expression for the asymptotic limit of infinite chain length is of similar quality to the numerical evaluation of Marko and Siggia's variational theory and considerably more precise than their interpolation formula. A comparison to numerical data suggests that our analytical finite chain length corrections achieve a comparable accuracy. As an application of our results, we discuss the possibility of inferring the time-dependent number of nicks in single-molecule stretching experiments on double-stranded DNA from the accompanying changes in the effective chain length.

I. INTRODUCTION

The wormlike chain (WLC)[1] is the standard model for describing the statistical physics of semiflexible polymers and is widely used in the context of biological physics to describe stiff cytoskeletal filaments such as actin or microtubules.[2–14] The present article is primarily motivated by the application of the WLC[15–17] to single-molecule experiments, where double-helical DNA,[15,18–22] proteins,[23] or polysaccharides[24] are stretched by an external force.

In their classical works, Marko and Siggia[15,16] showed that the original experiments of Smith, Finzi, and Bustamante[18] with λ-phage DNA are significantly better described by the WLC than by other polymer models (Fig. 1). While λ-phage DNA has a size of 48 kb or $N_p = L/l_p = 320$ persistence lengths, single-molecule stretching experiments can be carried out for much shorter segments.[27,28] From the point of view of theory, this leads to qualitative changes, which we have tried to illustrate in Fig. 2, where we show chain conformations and density distributions for the free chain-end positions. The different panels present results for a range of chain lengths [contour lengths L equal to 8, 40, 320 l_p persistence lengths corresponding to double-stranded DNA (ds-DNA) of 1.2 kb, 6 kb, 48 kb] and for two levels of the applied force [(a) $f = 0$ and

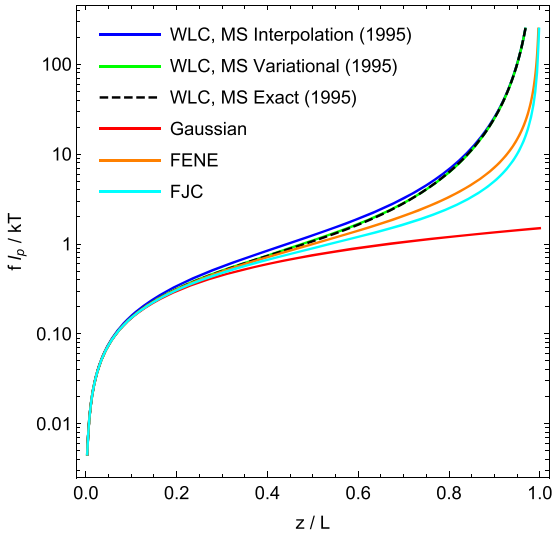

FIG. 1. Comparison of force–elongation curves for a number of popular polymer models discussed in the present article. The abbreviation FJC stands for the "freely jointed chain."[25]

(b) $f = k_BT/l_p$ = 4 pN nm/(50 nm) ≈ 0.1 pN, where ds-DNA is stretched to about half its maximal extension]. As in the force–elongation curves in Fig. 1, distances in Fig. 2 are scaled to the maximal chain extension L (indicated by the semi-transparent half sphere centered on the fixed chain end). With unperturbed end-to-end distances of $\sqrt{\langle r^2\rangle} = \sqrt{2l_pL}$ and $\sqrt{\langle (r/L)^2\rangle} \sim \sqrt{l_p/L}$, short chains exhibit substantial fluctuations in this representation. In contrast, long chains of the size of λ-phage DNA are hardly visible while unstretched and are almost perfectly aligned when they elongate in the direction of the applied force. In the (thermodynamic) limit of infinite chain length, the distributions of the end point positions shrink to a point: force–elongation and elongation–force relations become each other's inverse. Figure 2 illustrates Marko and Siggia's reasons for focusing on this limit, when they analyzed data for λ-phage DNA. However, a theoretical analysis of the behavior of shorter chains needs to take into account fluctuations and their different nature in the constant-force and constant-elongation ensembles.

To deal with this situation, we choose a different theoretical approach than Marko and Siggia's. Instead of *solving* the WLC model in the presence of a stretching force, we derive the response in the two ensembles from given expressions for the radial distribution

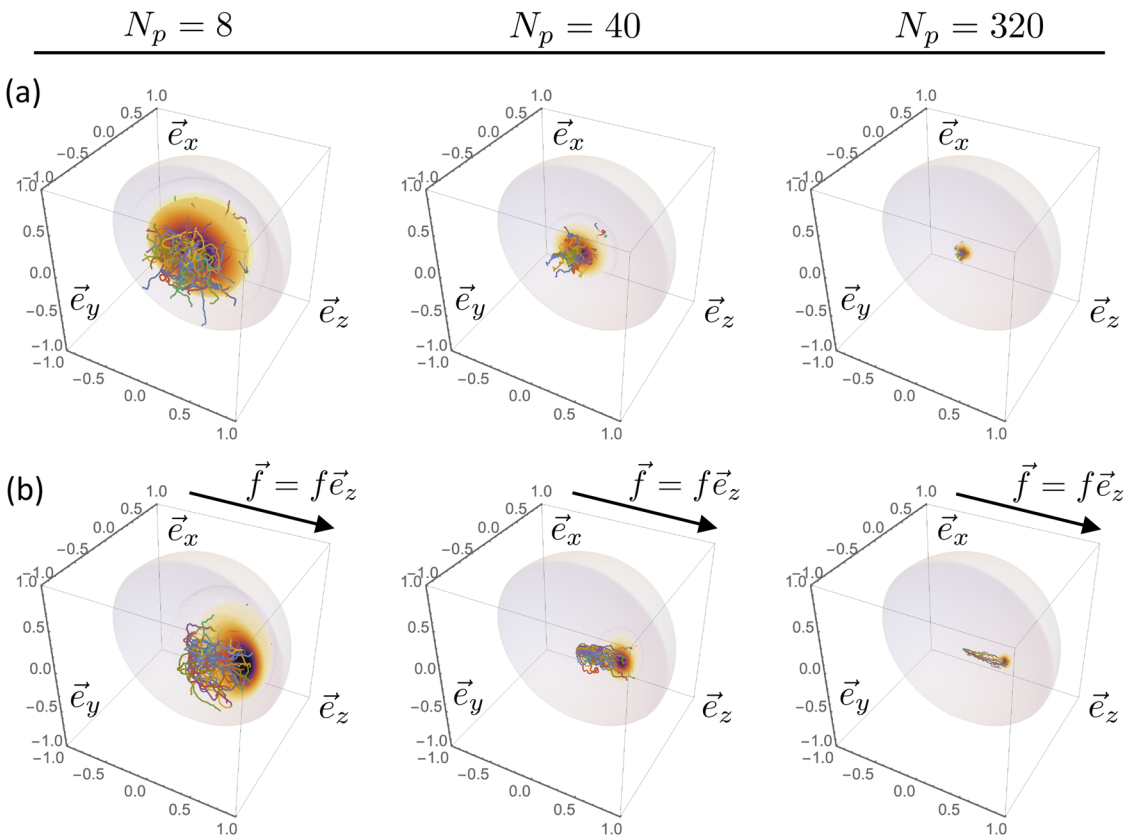

FIG. 2. Simulated chain conformations and chain-end density distributions predicted by the BRE-distribution from Ref. 26: results for three different chain lengths corresponding to single ds-DNA filaments of 1.2 kb, 6 kb, 48 kb. (a) Zero applied force, $f = 0$. (b) $f = k_BT/l_p$ = 4 pN nm/(50 nm) ≈ 0.1 pN, where ds-DNA is stretched to about half its maximal extension. Note that distances are scaled by the maximal chain extension L, which is indicated by the semi-transparent half sphere centered on the chain end fixed at the origin. Chain diameters are rescaled by a smaller factor because otherwise the longest chains would become invisible.

function of unperturbed polymer chains. This paper is organized as follows: In Sec. II, we briefly summarize the main features of the WLC model and the main results from the study of Marko and Siggia.[16] Sec. III is devoted to a systematic derivation of the elongation–force and force–elongation relations of long (wormlike) polymers from a given expression for the chain end-to-end distance distribution. In particular, we obtain analytical expressions for and gain insight into the finite chain length corrections in the two ensembles, where chains are held at constant force and constant elongation, respectively. In Sec. IV, we apply this formalism to a number of end-to-end distance distributions of polymer chains. As a first validation, we consider the exactly solvable cases of Gaussian springs and finitely extensible nonlinear-elastic (FENE)-springs. In the second step, we apply the formalism to two approximate expressions for the radial distribution function of the WLC. Bhattacharjee, Thirumalai, and Bryngelson (BTB)[29] derived a suitable expression using the variational theory of Ha and Thirumalai.[30,31] As an alternative, we (hereafter "BRE," see Ref. 26) proposed an interpolation between exact results for all relevant limiting cases of the WLC model ranging from short (stiff) to long (flexible) chains and including looped and fully stretched configurations. In Sec. V, we compare the resulting analytical expressions for the asymptotic force–elongation relation of "BTB"-springs and "BRE"-springs and the first-order corrections in both ensembles to analytical, numerical, and simulation results for long WLCs. In addition, we discuss the elastic response of the nicked WLC composed of several freely jointed wormlike segments. In this case, finite chain length effects turn out to be controlled by the average segment length. In particular, we show that, under suitable conditions, single-molecule stretching experiments of DNA should be able to detect enzyme-induced changes in the number of single-strand breaks. We briefly conclude in Sec. VI. For better readability, we have separated part of the material from the main text. Appendix A summarizes the simulation and data analysis methods we have used to obtain numerical reference data for FENE-springs, BTB-springs, and BRE-springs as well as for the WLC. Appendixes B–D report details on the derivation and interpretation of our analytic results for harmonic springs, FENE-springs, and BTB-springs.

II. BACKGROUND

A. The model

The WLC is defined via a Hamiltonian

$$\frac{\mathcal{H}_{\mathrm{WLC}}}{k_BT} = \frac{1}{2} l_p \int_0^L \left(\frac{\partial^2}{\partial s^2} \vec{r}(s) \right)^2 ds \tag{1}$$

for incompressible space-curves of contour length L with bending rigidity $l_p\ k_BT$, where l_p is the persistence length and k_BT is the thermal energy. Despite its simple appearance, the incompressibility constraint, $\left| \frac{\partial}{\partial s} \vec{r}(s) \right| \equiv 1$, renders the model non-trivial to solve. Notable exceptions[32] are the even moments $\langle r^{2k}(L) \rangle$ of the end-to-end distance r and, in particular ($k = 1$), the mean-square end-to-end distance[1] given by the formula

$$\langle r^2(L) \rangle \equiv \langle |\vec{r}(L) - \vec{r}(0)|^2 \rangle = 2 l_p^2 \left(\frac{L}{l_p} + e^{-L/l_p} - 1 \right). \tag{2}$$

This expression shows a crossover from rigid rod behavior, $\langle r^2(L) \rangle = L^2$, to random walk behavior, $\langle r^2(L) \rangle = 2 l_p L$, for contour lengths, L, around the persistence length, l_p.

Nature offers examples of polymers in a wide range of ratios L/l_p. For instance, cytoskeletal filaments such as microtubules[8] typically have $L \leq l_p$. In this work, we focus on chains, which are much longer than their persistence length, $L \gg l_p$ and $N_p \equiv L/l_p \gg 1$. This is, for example, the case in DNA stretching experiments.[16]

We are interested in two related mechanical problems, the force–elongation and the elongation–force relation of the freely rotating WLC. The former specifies the expectation value of the force, $\langle \vec{f}(z) \rangle = \langle f(z) \rangle \vec{e}_z$, required to constrain the projected elongation of a WLC to a constant value $z \equiv z(L) - z(0) = (\vec{r}(L) - \vec{r}(0)) \cdot \vec{e}_z$. The latter denotes the average elongation, $\langle z(f) \rangle$, of a WLC in the direction of a constant force, $\vec{f} = f \vec{e}_z$, separating its ends. That is, the average $\langle z(f) \rangle$ is taken with respect to the forced Hamiltonian

$$\mathcal{H} = \mathcal{H}_{\mathrm{WLC}} - f z. \tag{3}$$

B. DNA stretching

In their seminal analysis,[16] Marko and Siggia discussed the following *inter alia*: (1) the asymptotic behavior of the force in the limit of strong stretching

$$\lim_{z \to L} \frac{f}{k_BT/l_p} = \frac{1}{4(1 - z/L)^2}; \tag{4}$$

(2) an analytic expression (blue in Fig. 1),

$$\frac{f}{k_BT/l_p} = \frac{z}{L} + \frac{1}{4(1 - z/L)^2} - \frac{1}{4}, \tag{5}$$

interpolating from Eq. (4) to the opposite (random walk) limit of weak stretching

$$\lim_{z \to 0} \frac{f}{k_BT/l_p} = \frac{3}{2} \frac{z}{L}; \tag{6}$$

(3) a more precise variational calculation of the stretching force (green in Fig. 1); and (4) how to obtain the exact force–elongation relation with sufficient precision by numerically diagonalizing a 100×100 matrix (dashed black in Fig. 1). They noted that (3) and (4) were necessary because of the high quality of the experimental data.

Marko and Siggia worked in the constant-tension ensemble, since they were motivated[15] by the experiments of Smith *et al.*,[18] who attached one end of phage-λ DNA to a glass slide and the other to a magnetic bead on which they could exert a force. The complementary constant-elongation ensemble can be explored in atomic force microscope experiments,[28,33] where the mobile end of

the DNA molecule is attached to a cantilever, which probes the force needed to maintain an imposed constant displacement. The results of pulling experiments in the two ensembles are not expected to be equivalent for chains of finite contour lengths; that is, the force–elongation relation in the constant-force ensemble is not the inverse function of the elongation–force relation in the constant-elongation ensemble.[34–36] Below, we will consider both situations in turn (see Secs. III A and III B).

III. THEORY

In the present work, we infer the elastic properties of polymers from their end-to-end distance distribution,

$$Q(r) \equiv \frac{1}{4\pi r^2}\langle \delta(|\vec{r}(L) - \vec{r}(0)| - r)\rangle. \tag{7}$$

Without loss of generality, we consider a geometry where one chain end is fixed at the origin and where the rotational symmetry is broken either (i) by constraining the other chain end to a plane orthogonal to the z-direction or (ii) by applying a force $\vec{f} = f\vec{e}_z$ to the free chain end. The behavior in the constant-*elongation* ensemble [(i), to be discussed in Sec. III A] is controlled by the partition function, $\mathcal{Z}(z)$, defined as the integral of $Q(r)$ over the considered z-plane, Eq. (11). The average force, $\langle f(z)\rangle$, required to constrain the chain end to this plane is given by the z-derivative of the corresponding free energy, Eq. (13). By contrast, the statistical weight $w(z; f)$ of a particular z-elongation in the constant-*force* ensemble [(ii), to be discussed in Sec. III B] is given by the product of $\mathcal{Z}(z)$ and a force-dependent Boltzmann factor. Equation (39) defines the relevant partition function, $\mathcal{Z}(f)$, as the integral of $w(z; f)$ over all possible values of z. The expectation value $\langle z(f)\rangle$ follows from the normalized probability, $p(z;f) = w(z;f)/\mathcal{Z}(f)$, to observe a particular elongation, Eq. (41), and can equally be written as a force-derivative of the free energy, Eq. (42).

End-to-end distance distributions, $Q(r; L, l_p) = Q(r/L, l_p/L)$, and the partition function, $\mathcal{Z}(z; L, l_p) = \mathcal{Z}(z/L, l_p/L)$, can be written as a function of two dimensionless variables: the chain elongation in units of the maximal elongation,

$$\zeta = \frac{z}{L}, \tag{8}$$

and the (inverse) chain length in units of the bending persistence length,

$$\kappa = \frac{1}{N_p} = \frac{l_p}{L}. \tag{9}$$

We will focus on *long* chains, whose contour length exceeds the persistence length, $L \gg l_p$ or $\kappa \ll 1$ or $N_p \gg 1$. In this case, a useful dimensionless measure of the force is

$$\phi = \frac{f}{k_B T/l_p}. \tag{10}$$

We will alternate between the original and reduced variables as needed, throughout the text.

Below, we describe step by step how to infer the behavior of polymers in the two ensembles from given expressions for their end-to-end distance distribution, $Q(r/L, l_p/L)$. In particular, we will provide analytic expressions for the long-chain limit, $\kappa \to 0$, which are exact to first order in κ. Below, we briefly summarize the origin of the various terms and our notation to facilitate the reading.

For long chains, the partition function, $\mathcal{Z}(z)$, is dominated by the contribution $\mathcal{Z}_{(\cdot)}(z) = Q(z)$ from aligned chain conformations with $\vec{r} = (0, 0, z)$, see Fig. 3. In particular, the asymptotic force–elongation and elongation–force curves in the thermodynamic limit of infinite chain length can be immediately read off from the corresponding limit of $Q(z)$.

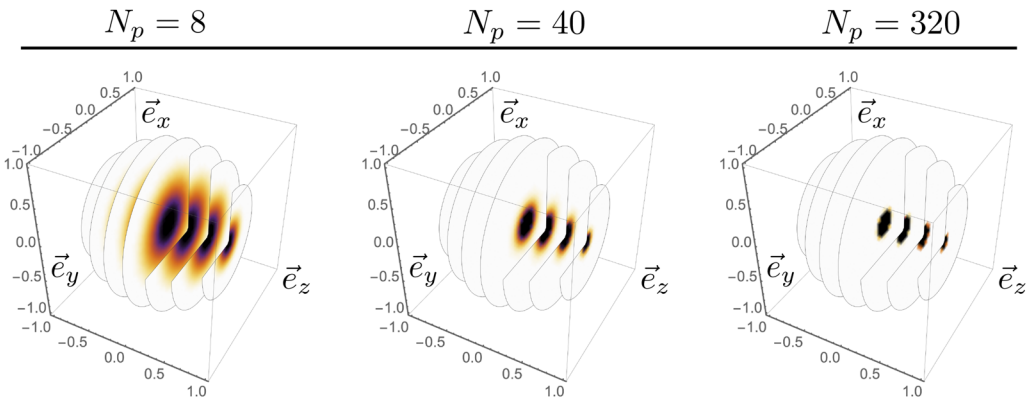

FIG. 3. The partition function $\mathcal{Z}(z)$ in the constant-elongation ensemble is defined as the integral of $Q(r = \sqrt{x^2 + y^2 + z^2})$ over a constant z-plane. For long chains, $\mathcal{Z}(z)$ is dominated by the contribution $\mathcal{Z}_{(\cdot)}(z) = Q(z)$ from aligned chain conformations with $\vec{r} = (0, 0, z)$. In the figure, we show the relative probability, $Q(\sqrt{x^2 + y^2 + z^2})/\mathcal{Z}_{(\cdot)}(z)$, to find the chain end at an off-center position in the same z-plane. The integral of this relative probability over the z-plane yields the partition function $\mathcal{Z}_{(\perp)}(z)$ for transverse fluctuations defined in Eq. (33). Note that the amplitude of transverse fluctuations decreases, when the z-extension of the chains approaches their maximal elongation.

In addition, we identify three qualitatively different finite chain length effects in single-molecule stretching experiments of long chains:

(i) "$\delta f_{(\cdot)}$" and "$\delta z_{(\cdot)}$" arising from finite chain length corrections to $Q(z)$;
(ii) "$\delta f_{(\perp)}$" and "$\delta z_{(\perp)}$" arising from the elongation-dependence of *transverse* fluctuations for a given value of z;
(iii) (in the constant-force ensemble, only) "$\delta z_{(\parallel)}$" arising from the elongation-dependence of the *longitudinal* fluctuations around the average extension $\langle z(f)\rangle$.

To first order in κ, corrections denoted "$\perp$" and "$\parallel$" only depend on the *asymptotic* limit of $Q(z)$ and are qualitatively similar for different chain models in the sense that the corresponding entropic springs become stiffer on approaching their maximal extension.

A. Force–elongation relations from end-to-end distance distributions

For chains whose free ends are constrained to a particular z-plane, the partition function is

$$\begin{aligned}\mathcal{Z}(z) &\propto \int d\vec{r}'\, Q(r')\delta(z'-z)\\ &\propto \int_0^{\sqrt{L^2-z^2}} d\rho\,\rho\, Q\Big(\sqrt{\rho^2+z^2}\Big).\end{aligned} \tag{11}$$

We define the potential of mean force as

$$\mathcal{F}(z) = -k_BT\log\mathcal{Z}(z), \tag{12}$$

so that the mean required constraining force is

$$\langle f(z)\rangle = \frac{d}{dz}\mathcal{F}(z) = -k_BT\,\frac{\mathcal{Z}'(z)}{\mathcal{Z}(z)}. \tag{13}$$

Without loss of generality, we consider chain ends constrained at $z>0$. As a consequence of our force convention, the constraining forces are also positive, $f>0$.

To proceed, we perform an analogous switch from the extensive free energy $\mathcal{F}$ to an intensive free energy $\mathcal{F}_p$ per persistence length,

$$\mathcal{F}(z;L,l_p) \equiv N_p\mathcal{F}_p(\zeta,\kappa), \tag{14}$$

$$\mathcal{F}_p(\zeta,\kappa) = -k_BT\log(\mathcal{Z}_p(\zeta,\kappa)), \tag{15}$$

$$\mathcal{Z}_p(\zeta,\kappa) \equiv \mathcal{Z}(z;L,l_p)^{\kappa}. \tag{16}$$

Using this notation, constraining forces can be computed as

$$\begin{aligned}\langle f(z;L,l_p)\rangle &= \frac{d}{dz}\mathcal{F}(z;L,l_p)\\ &= N_p\frac{d}{dz}\mathcal{F}_p(\zeta=z/L,\kappa)\\ &= \frac{1}{l_p}\mathcal{F}_p^{(1,0)}(\zeta,\kappa)\\ &= -\frac{k_BT}{l_p}\frac{\mathcal{Z}_p^{(1,0)}(\zeta,\kappa)}{\mathcal{Z}_p(\zeta,\kappa)},\end{aligned} \tag{17}$$

where we have introduced the notation $X^{(i,j)} \equiv \partial_\zeta^i\partial_\kappa^j X$ for quantities $X = X(\zeta,\kappa)$. Constraining forces can be directly expressed in the natural units of force, k_BT/l_p,

$$\langle\phi(\zeta,\kappa)\rangle \equiv \frac{\langle f(z;L,l_p)\rangle}{k_BT/l_p} = -\frac{\mathcal{Z}_p^{(1,0)}(\zeta,\kappa)}{\mathcal{Z}_p(\zeta,\kappa)} = -\kappa\frac{\mathcal{Z}^{(1,0)}(\zeta,\kappa)}{\mathcal{Z}(\zeta,\kappa)}. \tag{18}$$

1. Asymptotic behavior and finite-size corrections

For chains, which are much longer than their persistence length, $L\gg l_p$ and $N_p\gg 1$, the parameter $\kappa\ll 1$ can serve as a convenient expansion parameter for identifying the behavior close to the thermodynamic limit of infinitely long chains,

$$\mathcal{F}_p(\zeta,\kappa) = \mathcal{F}_p(\zeta) + \delta\mathcal{F}_p(\zeta,\kappa), \tag{19}$$

$$\delta\mathcal{F}_p(\zeta,\kappa) = \sum_{n=1}^{\infty}\frac{\kappa^n}{n!}\frac{d^n\mathcal{F}_p(\zeta,\kappa)}{d\kappa^n}\bigg|_{\kappa=0} \tag{20}$$

$$\equiv \sum_{n=1}^{\infty}\frac{\kappa^n}{n!}\mathcal{F}_p^{(0,n)}(\zeta,0). \tag{21}$$

Retaining the leading term

$$\mathcal{F}_p(\zeta) = -k_BT\log(\mathcal{Z}_p(\zeta,0)) \tag{22}$$

and corrections to first order in κ,

$$\delta\mathcal{F}_p(\zeta,\kappa) \approx \kappa\,\mathcal{F}_p^{(0,1)}(\zeta,0) \tag{23}$$

$$= -\kappa\,k_BT\frac{\mathcal{Z}_p^{(0,1)}(\zeta,0)}{\mathcal{Z}_p(\zeta,0)}, \tag{24}$$

the corresponding force–elongation relation reads

$$\langle\phi(\zeta,\kappa)\rangle = \phi(\zeta) + \delta\phi(\zeta,\kappa), \tag{25}$$

$$\phi(\zeta) = -\frac{\mathcal{Z}_p^{(1,0)}(\zeta,0)}{\mathcal{Z}_p(\zeta,0)}, \tag{26}$$

$$\delta\phi(\zeta,\kappa) \approx \kappa\left(-\frac{\mathcal{Z}_p^{(1,1)}(\zeta,0)}{\mathcal{Z}_p(\zeta,0)} + \frac{\mathcal{Z}_p^{(0,1)}(\zeta,0)}{\mathcal{Z}_p(\zeta,0)}\frac{\mathcal{Z}_p^{(1,0)}(\zeta,0)}{\mathcal{Z}_p(\zeta,0)}\right). \quad (27)$$

In particular, corrections are of the order $\delta f \sim \kappa\frac{k_BT}{l_p} = \frac{1}{N_p}\frac{k_BT}{l_p} = \frac{k_BT}{L}$.

2. Approximations

Since we are not always able to carry out the integrations in Eq. (11), we develop an approximation scheme valid for long chains, $L \gg l_p$ and $N_p \gg 1$, where $Q(r)$ is a monotonically decreasing function of distance.

Neglecting fluctuations, we may restrict the partition function to conformations with the minimal end-to-end distance, $r = z$, at the considered elongation in the z-direction. Denoting the partition function for chains with z-aligned end-to-end vectors by $\mathcal{Z}_{(\cdot)}$, we approximate

$$\mathcal{Z}(\zeta,\kappa) \approx \mathcal{Z}_{(\cdot)}(\zeta,\kappa) \propto Q(\zeta,\kappa). \quad (28)$$

With $\mathcal{Z}_{p,(\cdot)}(\zeta,\kappa) \propto Q_p(\zeta,\kappa)$, the corresponding zeroth and first order contributions to the restoring force can be directly read off from Eqs. (26) and (27),

$$\phi_{(\cdot)}(\zeta,\kappa) \equiv \phi_{(\cdot)}(\zeta) + \delta\phi_{(\cdot)}(\zeta,\kappa), \quad (29)$$

$$\phi_{(\cdot)}(\zeta) = -\frac{Q_p^{(1,0)}(\zeta,0)}{Q_p(\zeta,0)}, \quad (30)$$

$$\delta\phi_{(\cdot)}(\zeta,\kappa) \approx \kappa\left(-\frac{Q_p^{(1,1)}(\zeta,0)}{Q_p(\zeta,0)} + \frac{Q_p^{(0,1)}(\zeta,0)}{Q_p(\zeta,0)}\frac{Q_p^{(1,0)}(\zeta,0)}{Q_p(\zeta,0)}\right). \quad (31)$$

In the second step, we can approximate the integration over the transverse degrees of freedom by expanding $-k_BT\log\left(Q\left(\sqrt{\rho^2+\zeta^2},\kappa\right)\right) \approx -k_BT\log(Q(\zeta,\kappa)) + \frac{1}{2}k_{(\perp)}(\zeta,\kappa)\rho^2$, the linear contribution being absent because the displacement in the ρ-direction is perpendicular to the elongation in the z-direction. The coefficient of the second order term

$$k_{(\perp)}(\zeta,\kappa) = -k_BT\frac{\partial^2}{\partial\rho^2}\log\left(Q\left(\sqrt{\rho^2+\zeta^2},\kappa\right)\right)\Big|_{\rho=0} = -\frac{k_BT}{\zeta}\frac{Q^{(1,0)}(\zeta,\kappa)}{Q(\zeta,\kappa)} = \frac{f_{(\cdot)}(\zeta,\kappa)}{\zeta} \quad (32)$$

is the effective stiffness at the minimal elongation $r = z$ of chains constrained to a particular z-plane. Note that, independently of chain length, we are dealing with a single degree of freedom and that we are expanding (an approximation of) the extensive partition function, Q, and not Q_p. We remark that Eq. (32) is identical to the expression derived by Strick *et al.*[37] and used to measure the force f exerted on DNA molecules pulled by magnetic beads.

Extending the limits of the ρ-integration to infinity and carrying out the Gaussian integral,

$$\mathcal{Z}(\zeta,\kappa) \approx \mathcal{Z}_{(\cdot)}(\zeta,\kappa)\mathcal{Z}_{(\perp)}(\zeta,\kappa), \quad (33)$$

$$\mathcal{Z}_{(\perp)}(\zeta,\kappa) \propto \frac{1}{k_{(\perp)}(\zeta,\kappa)} \propto \frac{\zeta}{\phi_{(\cdot)}(\zeta,\kappa)}. \quad (34)$$

The change in the transverse fluctuations upon stretching makes an additive contribution to the restoring force,

$$\langle f(\zeta,\kappa)\rangle \approx f_{(\cdot)}(\zeta,\kappa) + f_{(\perp)}(\zeta,\kappa). \quad (35)$$

With $\phi_{(\perp)}(\zeta,\kappa) = -\kappa\frac{\mathcal{Z}_{(\perp)}^{(1,0)}(\zeta,\kappa)}{\mathcal{Z}_{(\perp)}(\zeta,\kappa)}$, Eq. (18), this contribution vanishes asymptotically,

$$\phi_{(\perp)}(\zeta,\kappa) \equiv \phi_{(\perp)}(\zeta) + \delta\phi_{(\perp)}(\zeta,\kappa), \quad (36)$$

$$\phi_{(\perp)}(\zeta) = 0, \quad (37)$$

so that the asymptotic force–elongation relation is given by $\phi_{(\cdot)}(\zeta)$ and Eq. (30). Furthermore, we may neglect corrections to $\phi_{(\cdot)}(\zeta)$ when evaluating

$$\delta\phi_{(\perp)}(\zeta,\kappa) \approx \kappa\left(\frac{\phi_{(\cdot)}^{(1,0)}(\zeta,\kappa)}{\phi_{(\cdot)}(\zeta,\kappa)} - \frac{1}{\zeta}\right) \approx \kappa\left(\frac{\phi_{(\cdot)}^{(1,0)}(\zeta)}{\phi_{(\cdot)}(\zeta)} - \frac{1}{\zeta}\right) \quad (38)$$

to first order in κ.

B. Elongation–force relations from end-to-end distance distributions

For chains stretched in the z-direction,

$$\mathcal{Z}(f) \propto \int d\vec{r}\, Q(r)\exp\left(\frac{fz}{k_BT}\right) = \int_{-L}^{L} dz\, \mathcal{Z}(z)\exp\left(\frac{fz}{k_BT}\right). \quad (39)$$

We define the potential of mean elongation as

$$\mathcal{G}(f) = -k_BT\log(\mathcal{Z}(f)), \quad (40)$$

so that

$$\langle z(f)\rangle = \frac{\int_{-L}^{L} dz\, \mathcal{Z}(z)\, z \exp\left(\frac{f z}{k_B T}\right)}{\int_{-L}^{L} dz\, \mathcal{Z}(z) \exp\left(\frac{f z}{k_B T}\right)} \tag{41}$$

$$= -\frac{d}{df}\mathcal{G}(f). \tag{42}$$

Again, we are not always able to carry out the integrations in Eqs. (39) and (41), which requires us to generalize the above approximation scheme to include fluctuations in the z-direction.

1. Finite-size corrections to the inverse of the asymptotic force–elongation relation

Given a force–elongation relation, $\langle f(z)\rangle$, approximate elongation–force relations, $\langle z(f)\rangle$, can be obtained from Eqs. (39) to (42) with the help of Laplace's method. Expanding the logarithmic integrand of $\mathcal{Z}(f)$ around $0 \le z^* \le L$ and noting that the derivatives obey $f^{(n-1)}(z^*) = \mathcal{F}^{(n)}(z^*)$,

$$\begin{aligned} -\frac{\mathcal{F}(z)}{k_B T} + \frac{f z}{k_B T} = &-\frac{\mathcal{F}(z^*)}{k_B T} + \frac{f z^*}{k_B T} + \left(-\frac{f(z^*)}{k_B T} + \frac{f}{k_B T}\right)(z - z^*) \\ &-\frac{1}{2}\frac{f'(z^*)}{k_B T}(z - z^*)^2 - \frac{1}{6}\frac{f''(z^*)}{k_B T}(z - z^*)^3 \\ &-\sum_{n=4}^{\infty}\frac{1}{n!}\frac{f^{(n-1)}(z^*)}{k_B T}(z - z^*)^n. \end{aligned} \tag{43}$$

The integrand develops a maximum at z^*, if the external force, $f = f(z^*) = \mathcal{F}'(z^*)$, is equal to the average force [see Eq. (13)] required to constrain the elongation to z^*. The second order term describes the longitudinal stiffness at this elongation with an effective spring constant of $k_{(\parallel)}(z^*) = \mathcal{F}''(z^*)/k_B T = f'(z^*)/k_B T$. The third order term gives rise to anisotropic fluctuations around z^*.

To a first approximation, which becomes exact in the asymptotic limit, one can neglect all terms beyond the linear order, $n = 1$,

$$\mathcal{Z}(f(z^*)) \approx \mathcal{Z}(z^*) \exp\left(\frac{f(z^*) z^*}{k_B T}\right), \tag{44}$$

$$\mathcal{G}(f) \approx \mathcal{F}(z^*) - f z^*. \tag{45}$$

While this trivially equates the elongation–force relation to the inverted force–elongation relation, i.e., in natural units,

$$\zeta\big(\phi(\zeta^*, \kappa), \kappa\big) \equiv \zeta^*, \tag{46}$$

we are still left with two problems. First, we are not necessarily able to invert a general, non-linear force–elongation relation in closed form: in such cases, we can still provide a parametric representation of the elongation–force curve. In particular, in the asymptotic limit of $\kappa = 0$, we can plot $\{\phi(\zeta^*), \zeta(\phi(\zeta^*)) \equiv \zeta^*\}$ for $0 \le \zeta^* \le 1$. Second, we need to convert our corrections, $\delta\phi(\zeta, \kappa)$, to the asymptotic force–elongation relation into corresponding corrections $\delta\zeta(\phi, \kappa)$ to the asymptotic elongation–force relation. As illustrated in Fig. 4, we may write to first order in κ,

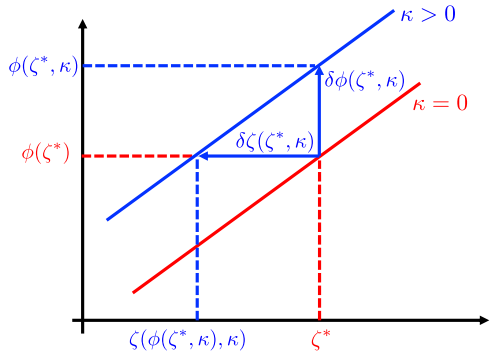

FIG. 4. "Geometric" derivation of Eqs. (47) and (48): conversion of the first-order correction, $\delta\phi(\zeta^*, \kappa)$, to the force–elongation relation, into the first-order correction, $\delta\zeta(\zeta^*, \kappa)$, to the inverse force–elongation relation.

$$\zeta\big(\phi(\zeta^*, \kappa), \kappa\big) = \zeta^* + \delta\zeta(\zeta^*, \kappa), \tag{47}$$

$$\delta\zeta(\zeta^*, \kappa) \approx -\frac{\delta\phi(\zeta^*, \kappa)}{\phi'(\zeta^*)}. \tag{48}$$

In particular,

$$\delta\zeta_{(\cdot)}(\zeta^*, \kappa) \approx -\frac{\delta\phi_{(\cdot)}(\zeta^*, \kappa)}{\phi'(\zeta)}, \tag{49}$$

$$\delta\zeta_{(\perp)}(\zeta^*, \kappa) \approx -\frac{\delta\phi_{(\perp)}(\zeta^*, \kappa)}{\phi'(\zeta)}. \tag{50}$$

2. Additional finite-size corrections

Higher order terms in Eq. (43) describe additional corrections, $\delta\zeta_{(\parallel)}(\zeta^*, \kappa)$, induced by longitudinal fluctuations,

$$\langle\zeta\big(\phi(\zeta^*, \kappa)\big)\rangle = \zeta^* + \delta\zeta_{(\cdot)}(\zeta^*, \kappa) + \delta\zeta_{(\perp)}(\zeta^*, \kappa) + \delta\zeta_{(\parallel)}(\zeta^*, \kappa). \tag{51}$$

To a second approximation, we retain the second order term in Eq. (43) and expand the exponential with the third order term to first order,

$$\begin{aligned} \mathcal{Z}(z) \exp\left(\frac{f(z^*) z}{k_B T}\right) \approx &\mathcal{Z}(z^*) \exp\left(\frac{f(z^*) z^*}{k_B T}\right) \exp\left(-\frac{1}{2}\frac{f'(z^*)}{k_B T}\delta z^2\right) \\ &\times\left(1 - \frac{1}{6}\frac{f''(z^*)}{k_B T}\delta z^3\right), \end{aligned} \tag{52}$$

when evaluating the integrals in Eqs. (39) and (41). Extending the integration range to infinity and noting that Gaussian integrals for

odd powers of δz vanish due to symmetry, the partition function for longitudinal fluctuations is given by

$$\mathcal{Z}_{(\parallel)}(f(z^*)) = \sqrt{\frac{2\pi k_B T}{f'(z^*)}}, \tag{53}$$

while

$$\delta z_{(\parallel)}(z^*) = -\frac{k_B T}{2}\frac{f''(z^*)}{(f'(z^*))^2}. \tag{54}$$

Note that the latter result can also be obtained by differentiating the corrected force-dependent free energy,

$$\mathcal{G}(f) = \mathcal{F}(z^*) - f z^* + \frac{k_B T}{2}\log\left(\frac{f'(z^*)}{k_B T}\right), \tag{55}$$

with respect to the applied force, Eq. (42). Rewriting in terms of dimensionless variables and to first order in κ,

$$\delta\zeta_{(\parallel)}(\zeta^*, \kappa) = \kappa\frac{\phi''(\zeta^*)}{2(\phi'(\zeta^*))^2}, \tag{56}$$

we see that this effect is of comparable magnitude to the other corrections in Eq. (51).

To summarize, we have identified three main contributions entering the first-order corrections to the asymptotic chain behavior: (1) from chain conformations whose end-to-end vectors are aligned along the z-direction [symbol $(\cdot)$]; (2) from chain conformations whose end-to-end vectors make "transverse" fluctuations, orthogonal to the prescribed z-direction [symbol $(\perp)$]; and (3) from chain conformations fluctuating along the z-direction, i.e., longitudinal fluctuations that are allowed *only* in the constant-force ensemble [symbol $(\parallel)$].

IV. RESULTS

Below and in Appendixes B–D, we report results obtained by applying the above formalism to four different expressions for the end-to-end distance distribution of polymer chains. All calculations can be performed exactly for Gaussian and finitely extensible nonlinear elastic (FENE) chains. While the former case provides a mere sanity check, the FENE model allows us to validate both, the theoretical analysis from Sec. III and the data analysis for our numerical results (Appendix A). For a systematic evaluation of the quality of available analytical expressions for the end-to-end distance distribution of the WLC, we refer the reader to Ref. 26. Here, we analyze the behavior of "BTB"-springs introduced by Bhattacharjee, Thirumalai, and Bryngelson[29] as well as "BRE"-springs defined via our own proposition for the radial distribution function of the WLC. To facilitate the comparison of the different systems in the two ensembles, Figs. 12 and 13 for FENE-springs in Appendix C, Figs. 14 and 15 for BTB-springs in Appendix D, and Figs. 5 and 6 for BRE-springs, as well as the final comparison to WLC data in Figs. 8 and 9, all follow identical outlines.

A. Gaussian chains

The ubiquitous[25] Gaussian chain model of polymer physics describes the conformations of long, $L \gg l_p$, non-interacting or ideal chains, whose radial distribution function follows a Gaussian distribution as long as $r \ll L$,

$$Q(r) \propto \exp\left(-\frac{3r^2}{4l_p L}\right) = \exp\left(-\frac{3}{4}N_p\left(\frac{r}{L}\right)^2\right). \tag{57}$$

The model is obviously exactly solvable and exhibits no finite-size corrections to the force–elongation and elongation–force relations, if the above expression is used for arbitrary values of r. Appendix B discusses the application of the formalism from Sec. III to Gaussian chains. In particular, we show that the exact behavior is identical to the asymptotic behavior inferred from the asymptotic partition function, $\mathcal{Z}_{p,(\cdot)}(z/L)$, per persistence length. Furthermore, the finite chain length corrections $\delta f_{(\cdot)}$ [Eq. (31)], $\delta f_{(\perp)}$ [Eq. (38)], and $\delta z_{(\parallel)}$ [Eq. (56)] are all identical to zero for harmonic springs.

B. FENE-springs

While it is reassuring to recover the well-known behavior of Gaussian chains, the model is too simple to provide a serious test of our approach. In Appendix C, we explore the behavior of finitely extensible non-linear elastic (FENE)-springs.[38] The radial distribution function for FENE-springs

$$\begin{aligned} Q\left(\frac{r}{L}, N_p\right) &\propto \exp\left(\frac{3}{4}N_p\log\left[1-\left(\frac{r}{L}\right)^2\right]\right) \\ &\propto \left(1-\left(\frac{r}{L}\right)^2\right)^{\frac{3}{4}N_p} \end{aligned} \tag{58}$$

reduces to the Gaussian distribution, Eq. (57), for $L \gg l_p$ as long as $r \ll L$. However, contrary to Gaussian chains, the partition function of FENE-springs drops to zero in the limit of full elongation, $r \to L$. As consequence, the contour length is a relevant independent length scale.

The FENE model was not derived from an underlying microscopic chain model but chosen for the relative ease with which it can be manipulated mathematically.[38] Conveniently, the model can also be solved exactly in the present context (Sec. C 1). This provides us with a non-trivial test case for our approximation scheme, which yields analytic expressions for the asymptotic behavior and the first order corrections due to transverse and longitudinal fluctuations. Notably, there are no finite chain length corrections to $Q(r)$ and, hence, $f_{(\cdot)}(z)$.

Figures 12 and 13 present a detailed analysis of the behavior of FENE-springs in the constant-elongation and constant-force ensembles, respectively. The results for the latter are shown with the dependent variable on the abscissa to simplify the comparison between the two ensembles. Besides the overall force–elongation and elongation–force relations [Figs. 12(a) and 13(a)] and the *relative* finite chain length correction, $\delta f(z)/f(z)$, to the former [Fig. 12(b)], we find (i) the difference between the inverted force–elongation relations for chains of finite length and the asymptotic elongation

force relation [Fig. 12(c)], (ii) the difference between the elongation–force relation and the inverted force–elongation relation for chains of a given length [Fig. 13(b)], and (iii) the difference between the elongation–force relations for chains of finite length and the asymptotic elongation–force relation [Fig. 13(c)], which is the sum of the first two terms. The comparison confirms the ability of our formalism to predict the asymptotic behavior (Sec. C 2) as well as the leading order finite chain length corrections to the force–elongation and elongation–force relations (Secs. C 3 and C 4, respectively).

Last but not least, the FENE model provides us with a stringent test case for validating the data analysis pipeline described in Appendix A (compare symbols to lines in Figs. 12 and 13).

C. "BTB-springs" representing long WLCs

In Ref. 29, Bhattacharjee, Thirumalai, and Bryngelson used a variational approach[30,31] to replace the hard incompressibility constraint $\left|\frac{\partial}{\partial s}\vec{r}(s)\right| = 1, \forall s \in [0, L]$ of the WLC with its thermal average $\langle(\frac{\partial}{\partial s}\vec{r}(s))^2\rangle = 1$ and derived the following approximate formula for the end-to-end distribution function of a WLC:

$$Q\left(\frac{r}{L}, N_p\right) \propto \left(1-\left(\frac{r}{L}\right)^2\right)^{-9/2} \exp\left(-\frac{3}{4}N_p\frac{1}{1-(r/L)^2}\right). \tag{59}$$

In Appendix D, we explore the properties of the corresponding BTB-springs. As for FENE-springs, we can calculate their asymptotic behavior to first order in $\kappa = 1/N_p$ using the approximation scheme outlined in Sec. III. In this case, the finite chain length corrections to $Q(r)$ are relatively strong. Compared to the correction $\delta f_{(\perp)}(z)$ from transverse fluctuations, $\delta f_{(\cdot)}(z)$ is about twice as large and of the *opposite* sign. In particular, the BTB distribution implies that, for the WLC, $\delta z_{(\cdot)}(z)$ should nearly cancel the sum of $\delta z_{(\perp)}(z)$ and $\delta z_{(\parallel)}(z)$ in the constant-force ensemble.

Figures 14 and 15 for BTB-springs are the exact analogs of Figs. 12 and 13 for FENE-springs, which we have discussed in Sec. IV B. In all cases, our numerical results for BTB-springs are in excellent agreement with the results of this analysis with the predicted asymptotic behavior and theoretically expected first order corrections to the force–elongation and elongation–force relations.

D. "BRE-springs" representing long WLCs

In Ref. 26, we have proposed a closed analytical expression

$$Q_{\mathrm{BRE}}(r) \equiv (1-cr^2)^{5/2}\, Q_A(r)\, Q_B(r) \tag{60}$$

for the end-to-end distance distribution of the WLC composed of three factors, which interpolates between all relevant limiting cases from stiff to flexible chains and from looped to fully stretched configurations. By analogy to the FENE-case, $\mathcal{F}_{\mathrm{BRE}}(r) = -k_BT\log(Q_{\mathrm{BRE}}(r))$ describes the elastic (free) energy of a nonlinear, finite-extensible spring. In order to keep both notation and terminology concise, we will refer to corresponding results as describing the behavior of "BRE-springs."

In the context of DNA stretching, we are mostly interested in chains, which are much longer than their persistence length, $L \geq 8l_p$. In this case, $c \approx 0$ and $Q_B(r) \propto 1$, and we can extract all distance dependent factors of the radial distribution function from

$$Q_A(r) \propto \left(1-\left(\frac{r}{L}\right)^2\right)^{-5/2} \exp\left(\frac{-\frac{1}{2}\left(\frac{r}{L}\right)^2+\frac{17}{16}\left(\frac{r}{L}\right)^4-\frac{9}{16}\left(\frac{r}{L}\right)^6}{1-\left(\frac{r}{L}\right)^2}\right)$$
$$\times \exp\left(\frac{-\frac{3}{4}\left(\frac{r}{L}\right)^2+\frac{23}{64}\left(\frac{r}{L}\right)^4-\frac{7}{64}\left(\frac{r}{L}\right)^6}{1-\left(\frac{r}{L}\right)^2}\frac{L}{l_p}\right), \tag{61}$$

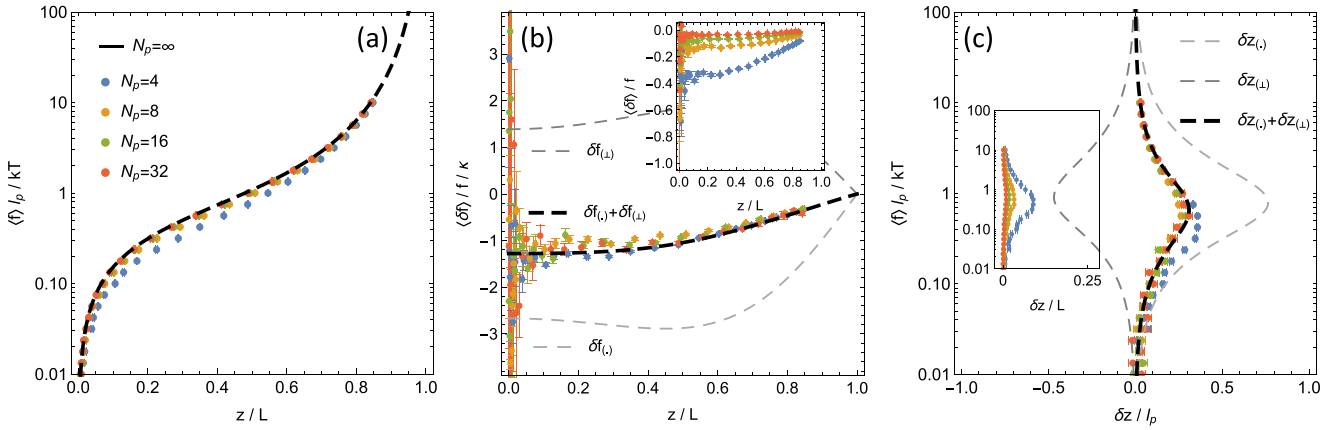

FIG. 5. BRE-springs in the constant-elongation ensemble: (a) force–elongation relations, (b) finite-size corrections $[\langle\delta f\rangle \equiv \langle f(z,\kappa)\rangle - \langle f(z,\kappa=0)\rangle]$ to the force–elongation relation, and (c) finite-size corrections $[\delta z \equiv \langle f(z,\kappa)\rangle^{-1} - \langle f(z,\kappa=0)\rangle^{-1}]$ to the inverted force–elongation relation. The insets show finite-size corrections in the units of the force–elongation relation, while the main panels show rescaled results in comparison with the theoretical expressions for the leading order term. Symbols represent the most likely elongation of BRE-springs in MC simulations in the constant-*force* ensemble (see Sec. A 3).

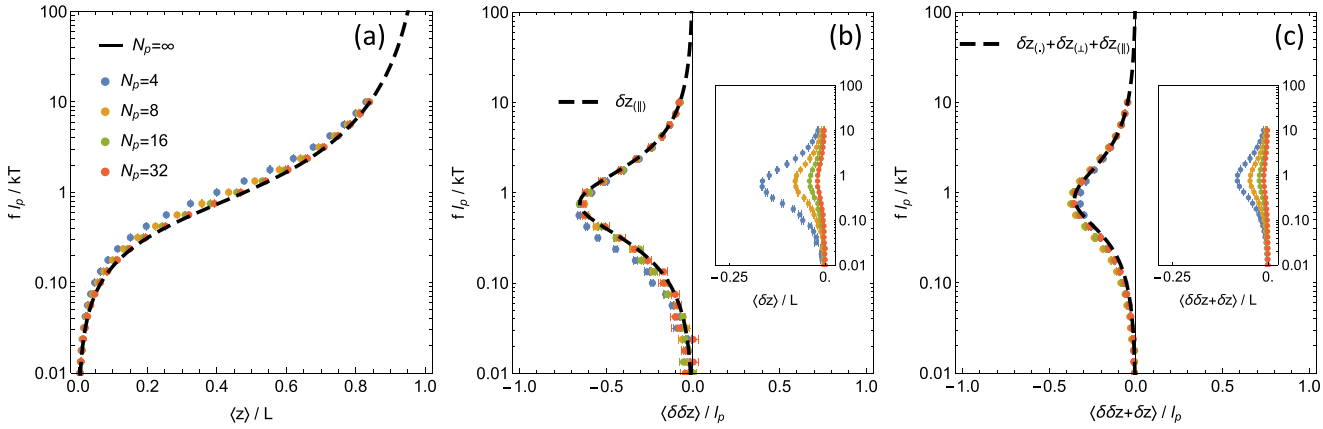

FIG. 6. BRE-springs in the constant-force ensemble: (a) elongation–force relations, (b) finite-size corrections $[\langle\delta\delta z\rangle \equiv \langle z(f,\kappa)\rangle - \langle f(z,\kappa)\rangle^{-1}]$ to the inverted force–elongation relations for chains of the same length, and (c) finite-size corrections $[\langle\delta\delta z + \delta z\rangle = \langle z(f,\kappa)\rangle - \langle z(f,\kappa=0)\rangle]$ to the asymptotic elongation–force relation. Symbols represent the average elongation of BRE-springs in MC simulations in the constant-force ensemble (see Sec. A 1). Note that all results are shown with the dependent variable on the abscissa to simplify the comparison with Fig. 5.

which we obtained[26] by a systematic interpolation between the exact limit results by Daniels[39] and Wilhelm and Frey.[40]

As in the case of BTB-springs, we first explore the properties of BRE-springs as such. Figures 5 and 6 for BRE-springs are the exact analogs of Figs. 12 and 13 for FENE-springs and Figs. 14 and 15 for BTB-springs. Again, we have not been able to obtain an exact analytic solution. As a consequence, we are restricted to validating results obtained from the approximation scheme outlined in Sec. III via a comparison with numerical data from Monte Carlo simulations of stretched BRE-springs. For a comparison of BRE-springs to the WLC, see Sec. V and Figs. 8 and 9.

1. Asymptotic behavior

In the asymptotic limit, the free energy per persistence length is given by the dominant exponential term in Eq. (61),

$$\frac{\mathcal{F}_{p,(\cdot)}(z/L)}{k_BT} = -\frac{-\frac{3}{4}(z/L)^2 + \frac{23}{64}(z/L)^4 - \frac{7}{64}(z/L)^6}{1-(z/L)^2}.$$

Differentiating with respect to the elongation, Eq. (30), yields

$$\frac{f_{(\cdot)}(z/L)}{k_BT/l_p} = \frac{1}{2}\frac{z}{L} + \frac{z/L}{(1-(z/L)^2)^2} - \frac{7}{16}\left(\frac{z}{L}\right)^3 \tag{62}$$

for the asymptotic force–elongation relation of BRE-springs. The behavior is similar to BTB-springs and largely dominated by the first two terms, which reproduce the exactly known behavior of the WLC in the two limits of weak and strong elongations, Eqs. (4) and (6), respectively. With the inverse, $z_{(\cdot)}(f)$, being the root of a seventh order polynomial, we show results in the constant-force ensemble as parametric plots.

2. Finite chain length corrections to the force–elongation relation

As in the other cases, the effective spring constant, Eq. (32), for transverse fluctuations of BRE-springs,

$$k_{(\perp)}(z/L) \propto \frac{1}{2} + \frac{1}{(1-(z/L)^2)^2} - \frac{7}{16}\left(\frac{z}{L}\right)^2, \tag{63}$$

diverges on approaching full elongation. To first order in κ, the corresponding finite-size correction, Eq. (38), for the force–elongation curve reads

$$\frac{\delta f_{(\perp)}(z/L,\kappa)}{k_BT/l_p} = \kappa\,\frac{\frac{z}{L}\left(\frac{4}{(1-(z/L)^2)^3} - \frac{7}{8}\right)}{\frac{1}{2} + \frac{1}{(1-(z/L)^2)^2} - \frac{7}{16}\left(\frac{z}{L}\right)^2}. \tag{64}$$

While the effect of transverse fluctuations is qualitatively similar in all three cases [panel (b) in Figs. 12, 14, and 5], the corrections for BRE-springs are somewhat smaller than those for BTB-springs.

Similarly to BTB-springs, BRE-springs exhibit finite-size corrections to the dominant free energy contribution, $\mathcal{F}_{p,(\cdot)}(z/L,\kappa)$, from aligned chains with the minimal elongation, $r = z$. Again, there is no explicit chain length dependence of the two subdominant factors in Eq. (61). As a consequence, there are no higher order corrections to $\delta\mathcal{F}_{p,(\cdot)}(z/L,\kappa)$ beyond the linear term,

$$\frac{\delta\mathcal{F}_{p,(\cdot)}(z/L,\kappa)}{k_BT} = \kappa\left(\frac{5}{2}\log\left(1-(z/L)^2\right) - \frac{-\frac{1}{2}(z/L)^2 + \frac{17}{16}(z/L)^4 - \frac{9}{16}(z/L)^6}{1-(z/L)^2}\right). \tag{65}$$

The corresponding correction, Eq. (31), to the elastic response reads

$$\frac{\delta f_{(\cdot)}(z/L,\kappa)}{k_BT/l_p} = \kappa\left(\frac{z}{L} - 5\frac{z/L}{1-(z/L)^2} - \frac{9}{4}\left(\frac{z}{L}\right)^3\right). \tag{66}$$

Note that the dominant FENE-like term in Eq. (66) has again the opposite sign from Eq. (C11). As for BTB-springs, the diverging subdominant factor of $\left(1-\left(\frac{r}{L}\right)^2\right)^{-5/2}$ in Eq. (61) *reduces* the drop in $Q_A(r)$ on approaching full elongation. Because of the smaller exponent, this correction is again smaller for BRE-springs than for BTB-springs.

For BRE-springs, the sum of the two corrections is approximately given by the more readable expression

$$\frac{\delta f(z/L,\kappa)}{k_BT/l_p} \approx \kappa\left(\frac{1}{2} - \frac{1}{2(1-z/L)} - \frac{17}{12}\frac{z}{L}\right). \tag{67}$$

While the total correction is qualitatively similar to the one for BTB-springs, it turns out to be only about half as strong. Compared to FENE-springs, the major difference is again the opposite sign caused by $\delta f_{(\cdot)}(z/L, \kappa)$. Our numerical results for BRE-springs are in excellent agreement with the results of this analysis [Fig. 5(b)].

3. Finite chain length corrections to the elongation–force relation

In the constant-elongation ensemble, we expect a correction due to the elongation-dependence of longitudinal fluctuations because the corresponding effective spring constant,

$$k_{(\parallel)}(z/L) \propto \frac{f'_{(\cdot)}(z/L)}{k_BT/l_p} \tag{68}$$

$$= \frac{1}{2} + \frac{1+3(z/L)^2}{(1-(z/L)^2)^3} - \frac{21}{16}\left(\frac{z}{L}\right)^2, \tag{69}$$

diverges even more rapidly than $k_{(\perp)}(z/L)$. For BRE-springs, Eq. (56) reads

$$\frac{\delta z_{(\parallel)}(z^*/L,N_p)}{L} = 48\kappa(z^*/L)\left(1-(z/L)^2\right)^2 \times \frac{-25-60(z^*/L)^2+42(z^*/L)^4-28(z^*/L)^6+7(z^*/L)^8}{\left(24+3(z^*/L)^2+87(z^*/L)^4-71(z^*/L)^6+21(z^*/L)^8\right)^2} \tag{70}$$

and can be approximated as

$$\frac{\delta z_{(\parallel)}(z^*/L,N_p)}{L} \approx \frac{l_p}{2L}\Bigg/\sqrt{\left(\frac{6}{25}\frac{L}{z^*}\right)^2+\left(\frac{1}{6}\frac{1}{(1-z^*/L)^2}\right)^2}. \tag{71}$$

The behavior shown in Fig. 6(b) is very similar to the results for the other cases. Again, our numerical results converge to the theoretical prediction.

Following the discussions in Sec. III B, we need to add $\delta z_{(\parallel)}$ to the finite chain length corrections from the inverted force–elongation relation given by Eqs. (49) and (50). With $\delta f_{(\perp)}$, $\delta f_{(\cdot)}$, and $f'_{(\cdot)}$ for BRE-springs defined in Eqs. (64), (66), and (68), the expressions

$$\frac{\delta z_{(\perp)}(z^*/L,\kappa)}{L} = -\frac{\delta f_{(\perp)}(z^*/L,\kappa)}{f'_{(\cdot)}(z^*/L)}, \tag{72}$$

$$\frac{\delta z_{(\cdot)}(z^*/L,\kappa)}{L} = -\frac{\delta f_{(\cdot)}(z^*/L,\kappa)}{f'_{(\cdot)}(z^*/L)} \tag{73}$$

gain little in being written out in full. The two functions are shown in Fig. 5(c). Like in the other cases, the corrections are strongest around $z/L \approx 1/2$ and $fl_p/k_BT \approx 1$. As for BTB-springs, $\delta z_{(\cdot)}$ and $\delta z_{(\perp)}$ have opposite signs. However, with $\delta z_{(\cdot)}$ being smaller, the sum, $\delta z_{(\cdot)} + \delta z_{(\perp)}$, is about 50% smaller. Again, the numerical results for BRE-springs are in excellent agreement with our analysis results.

The total finite chain length corrections to the elongation–force relation of BRE-springs are shown in Fig. 6(c). The first point to note is again the excellent agreement between the results of our simulations for chains with length $N_p = 4, \ldots, 32$ persistence lengths and the theoretically predicted first order correction, $\delta z_{(\cdot)} + \delta z_{(\perp)} + \delta z_{(\parallel)}$. Higher order terms appear to be negligible. A second key feature is revealed in the direct comparison to Figs. 13(c) and 15(c) for FENE-springs and BTB-springs: due to the magnitude and opposite sign of the contribution $\delta z_{(\cdot)}$, the total finite chain length corrections to the elongation–force relation of BRE-springs are surprisingly small, even though they do not exhibit the near cancellation we found in the case of BTB-springs.

V. DISCUSSION

In the present paper, we have developed a formalism for inferring force–elongation and elongation–force relations for single-molecule stretching experiments from given (approximate) expressions for the chain end-to-end distance distribution. We have validated the formalism for the analytically exactly solvable case of FENE-springs (Appendix C). In Appendix D and Sec. IV D, we have derived the relevant expressions for the approximate BTB-distributions and BRE-distributions for long WLCs, whose contour length is much larger than their persistence length, $L/l_p = N_p \gg 1$.

We now turn to the question regarding which (if any) of the approximate radial distribution functions allows us to derive a quantitative description of the behavior of wormlike chains. We will follow the same outline as in Secs. IV A, IV B, IV C, and IV D. In Sec. V A, we compare the asymptotic force–elongation relation of BTB-springs and BRE-springs to the results of Marko and Siggia. In the second step (Sec. V B), we use our numerical results for the WLC to test the corresponding expressions for the finite chain length corrections. As a final point, we show in Sec. V C how experimentalists might employ our results to infer the changing number of nicks in

a ds-DNA molecule by observing the changing mean elongation in a single-molecule stretching experiment, where the DNA is held at constant force.

A. Asymptotic behavior of WLC

In Fig. 7, we compare the asymptotic force–elongation relation for BTB-springs and BRE-springs, Eqs. (D1) and (62), to the MS approximate expression, Eq. (5), the numerical solution of the MS variational theory, an analytical expression proposed by Vologodskii [Eq. (4) in Ref. 19], the exact MS solution obtained by numerically inverting a 100 × 100 matrix, and an empirical formula by Bouchiat *et al.* [Eq. (11) in Ref. 20], who fitted a seventh order polynomial to the difference between the exact solution and Eq. (5). Considered over the full force and elongation range in panel (a), all approximate expressions provide a good approximation to the exact solution (indicated by a dashed black line). Only for Eq. (D1), the deviations are immediately apparent.

For a more detailed analysis, we have calculated the relative error of the asymptotic force–elongation relations [panel (b)] and the absolute error of the asymptotic elongation–force relations [panel (c)]. These representations show that the deviations of the BRE-spring expression, Eq. (62), are of the order of 2% over the full range of elongations. They are, thus, about one order of magnitude smaller than those for the MS approximation, Eq. (5), and comparable to the numerical evaluation of the MS variational theory. Vologodskii's expression is three to five times worse in the intermediate force regime and breaks down in both limits.[20] For BTB-springs, the elastic response to large forces is off by a factor of 3/2.[31] While Bouchiat *et al.*'s[20] fit of the exact MS solution retains its utility for the analysis of experimental data, Eq. (62) has at least the merit of being the most precise explicit expression resulting from a systematic theoretical approach to the problem.

B. Finite chain length effects for WLC

In the absence of exact results for the finite chain length corrections to the force–elongation and elongation–force relations of the WLC, we are limited to comparing the predictions we have derived from the BTB-distributions and BRE-distributions to our numerical data for the WLC. In order not to confuse the errors in the inferred asymptotic force–elongation relations with the predicted finite chain length corrections, we calculate the latter for our WLC data relative to the exact asymptotic MS force–elongation relation.

The presentation of our results in Figs. 8 and 9 is the exact analog of Figs. 14 and 15 for BTB-springs and of Figs. 5 and 6 for BRE-springs. The only difference is that symbols now represent simulation results for the WLC, while gray and black dashed lines represent predictions for BTB-springs and BRE-springs, respectively. In the constant-force ensemble, there is excellent agreement between the WLC data and the finite chain length corrections inferred from the BRE-distribution. In contrast, the BTB-results—while qualitatively perfectly reasonable—are off by a factor of 2–3 over the entire range of elongations [Figs. 8(b) and 8(c)]. We tentatively conclude that the predicted asymptotic force–elongation relations and finite chain length corrections seem to be of comparable quality. In the constant-elongation ensemble, there is very good agreement between the observed corrections due to longitudinal fluctuations and the predictions from both models [Fig. 9(b)]. However, due to the subtle cancellation effects, the total correction [Fig. 9(c)] is only correctly predicted by BRE-springs.

Curiously, for the WLC and BRE-springs, the average of the force–elongation and the elongation–force relation for chains of finite length appears to be an excellent estimator for the asymptotic force–elongation curve [panel (a) in Figs. 5 and 6 as well as Figs. 8 and 9, or even more clearly the corresponding panel (c)]. While this might be intuitively plausible, it is easy to show that the identity for BRE-springs is only approximate, but not exact. Moreover, the examples of FENE-springs and BTB-springs would

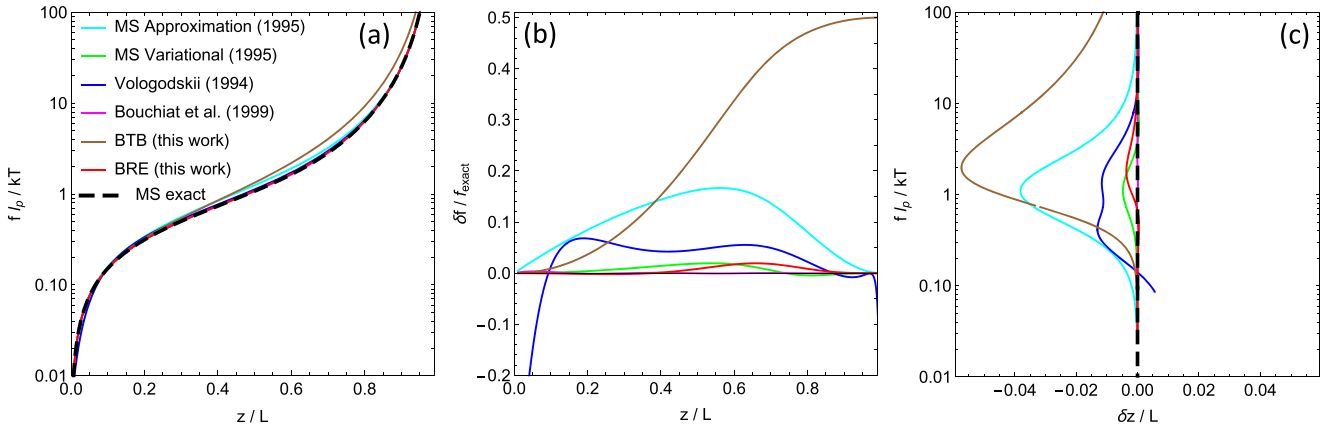

FIG. 7. (a) Asymptotic force–elongation relation for the WLC, (b) relative error of predicted forces, and (c) error of the predicted position. Black line: Marko and Siggia's exact solution. Cyan line: Marko and Siggia's approximate expression [Eq. (5)]. Green line: numerical solution of the Marko and Siggia variational theory. Blue line: Vologodskii's approximate expression.[19] Magenta line: Bouchiat *et al.*'s approximate expression.[20] Brown and red lines: analytical expressions, Eqs. (D1) and (62), derived from the BTB[29] and BRE[26] distributions.

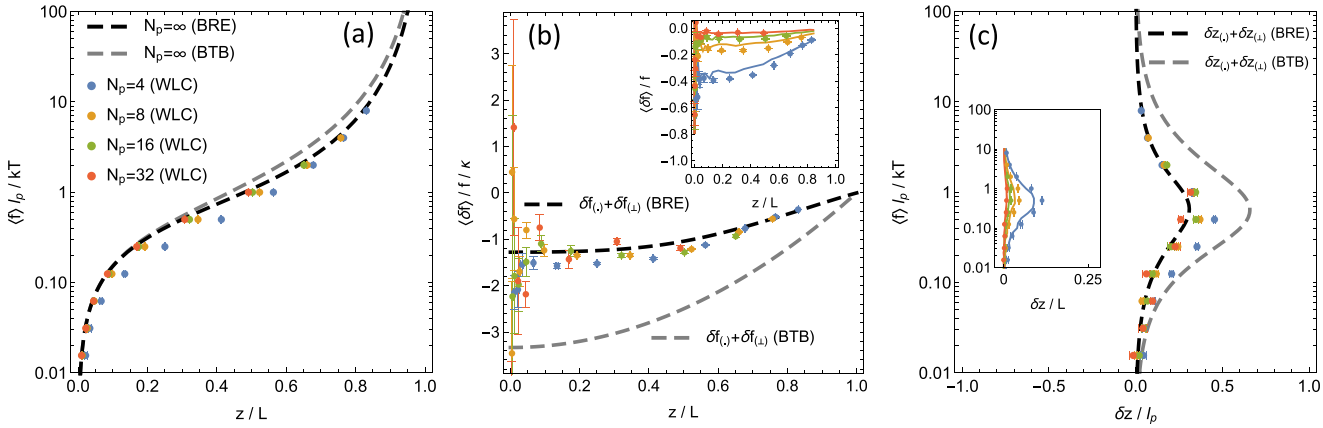

FIG. 8. WLC of finite length compared to corresponding BTB-springs and BRE-springs in the constant-elongation ensemble: (a) force–elongation relations, (b) finite-size corrections to the force–elongation relation, and (c) finite-size corrections to the inverted force–elongation relation. Symbols: most likely elongations of the WLC in MC simulations in the constant-*force* ensemble (see Sec. A 3). Gray dashed lines: theoretical results for BTB-springs (see Fig. 14). Black dashed lines: theoretical results for BRE-springs (see Fig. 5). Solid colored lines in the insets: numerical results for BRE-springs representing the WLC of finite length (see Fig. 5). Colors distinguish chain lengths, and label notation is as in Fig. 5.

seem to indicate that this near identity is an accident rather than a rule [Figs. 12(c) and 13(c) as well as Figs. 14(c) and 15(c)]. The corrections $\delta\zeta_{(\perp)}$ and $\delta\zeta_{(\parallel)}$ due to transverse and longitudinal fluctuations only depend on the asymptotic force elongation relation, $\phi_{(\cdot)}(\zeta)$. For reasonable polymer models, these corrections plausibly have a universal sign because their origin is the relative stiffening of the springs on approaching their maximal elongation. The different behavior of FENE-springs, BTB-springs, and BRE-springs is due to the first order correction, $\delta\phi_{(\cdot)}(\zeta)$, which arises from the dominant contribution to the partition function from chain conformations with the minimal total elongation, $r = z$, at the considered projected elongation. While this term vanishes for FENE-springs, for BTB-springs and BRE-springs, it counteracts and largely cancels the fluctuation-induced corrections.

C. Counting nicks in single-molecule stretching experiments of DNA

As an interesting application of our results, we discuss in the following the possibility to follow a dynamically changing number

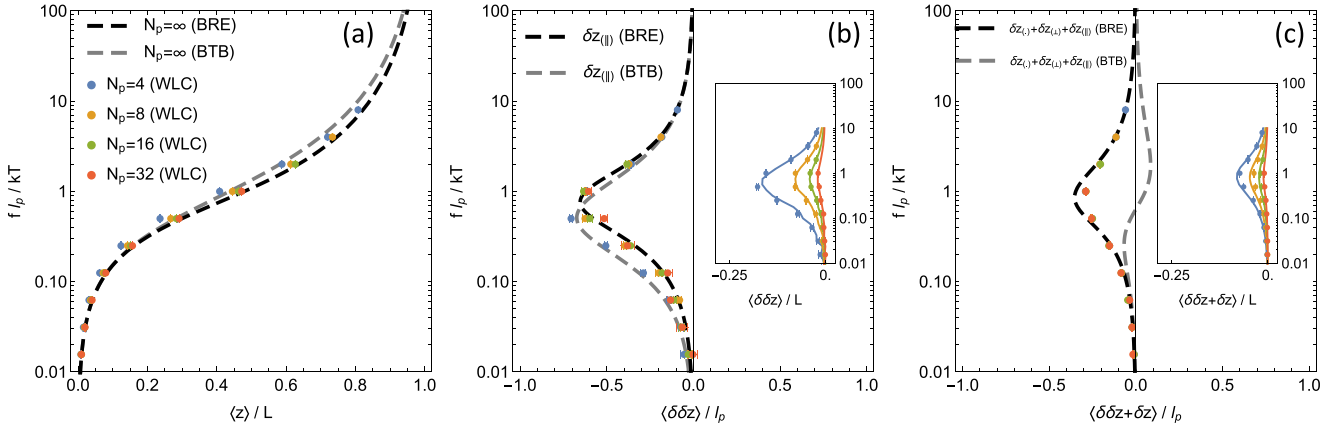

FIG. 9. WLC of finite length compared to corresponding BTB-springs and BRE-springs in the constant-force ensemble: (a) elongation–force relations, (b) finite-size corrections to the inverted force–elongation relations for chains of the same length, and (c) finite-size corrections to the asymptotic elongation–force relation. Symbols: average elongation of the WLC in MC simulations in the constant-force ensemble (see Sec. A 2). Gray dashed lines: theoretical results for BTB-springs (see Fig. 15). Black dashed lines: theoretical results for BRE-springs (see Fig. 6). Solid colored lines in the insets: numerical results for BRE-springs representing the WLC of finite length (see Fig. 6). Colors distinguish chain lengths, and label notation is as in Fig. 6.

of "nicks" in a molecule held at constant force by analyzing the accompanying changes in the average elongation. For DNA, such a situation may arise in the presence of enzymes, which can induce and repair single-chain breaks.

Consider a defect-free ds-DNA segment of length L under the influence of a dimensionless stretching force, ϕ. Retaining finite chain length effects to first order, its average elongation is given by

$$\langle z \rangle \equiv L\zeta(\phi) + l_p \delta_\zeta(\phi), \tag{74}$$

where $\delta_\zeta(\phi) = \lim_{\kappa\to 0}\delta\zeta(\phi,\kappa)/\kappa$. This expression is straightforward to generalize to the situation, where the molecule is composed of n *freely jointed* defect-free segments of a total length of $L = \sum_{i=1}^{n} L_i$,

$$\langle z \rangle = \sum_{i=1}^{n} \big(L_i \zeta(\phi) + l_p \delta_\zeta(\phi) \big) \tag{75}$$

$$= L\zeta(\phi) + n l_p \delta_\zeta(\phi). \tag{76}$$

The above relation has a number of interesting implications: (i) changing the number, $n-1$, of nicks by one changes the average chain elongation by a distance of the order of the DNA persistence length of $l_p = 50$ nm and (ii) this change depends neither on the total length, L, of the molecule nor on the precise position of the nicks. Note, however, that by equating a single-strand break to a free hinge, we have neglected the possibility that the double helix can remain stacked at the nick position.[41] Such a "passive" nick leaves the chain locally smooth and would be difficult to discern in single-molecule stretching experiments. Here, we focus on the detection of "active" nicks and leave the inclusion of "passive" nicks via a (sequence-and force-dependent) two-state model to future work.

Defining our usual parameter $\kappa = l_p/L$ for the known *total* contour length and rewriting Eq. (76) in terms of the expectation value of the reduced elongation, we obtain an elongation–force relation,

$$\left\langle \frac{z}{L} \right\rangle_n = \zeta(\phi) + n\kappa\, \delta_\zeta(\phi), \tag{77}$$

of the form that we have considered throughout this article. In particular, the introduction of a single nick *doubles* the finite chain length effects. Assuming that Eqs. (76) and (77) are borne out in experiments of DNA-molecules with a well-controlled number of nicks, we can invert the logic and *count* (active) nicks in single-molecule stretching experiments,

$$n = \frac{\left\langle \frac{z}{L} \right\rangle - \zeta(\phi)}{\kappa\, \delta_\zeta(\phi)}. \tag{78}$$

With the above caveats, Eq. (78) applies to a static setting. In contrast, if the nick dynamics is fast, one is bound to measure a response corresponding to the average number, $\langle n \rangle$, of freely jointed WLC segments.

To resolve dynamic changes in the number of nicks, one needs to measure $\left\langle \frac{z}{L} \right\rangle$ in between changes with sufficient precision to be able to distinguish the "quantized" mean elongations described by Eq. (77). To understand how this can best be achieved, we need to analyze the fluctuations.

Similarly to the total elongation, which is given by the sum of the subchain elongations, the variance of the total elongation is given by the sum of the variances of the subchain elongations. To zeroth order in κ, Eq. (68) implies that

$$\langle \delta z^2 \rangle = \frac{l_p}{\phi'(\zeta^*(\phi))} \sum_{i=1}^{n} L_i = \frac{l_p L}{\phi'(\zeta^*(\phi))}. \tag{79}$$

In particular, the distribution of instantaneous chain elongations for a WLC with $n-1$ (active) nicks is given by

$$p(z) = \frac{1}{\sqrt{2\pi\langle \delta z^2 \rangle}} \exp\left(-\frac{(z - \langle z \rangle_n)^2}{2\langle \delta z^2 \rangle} \right). \tag{80}$$

With the standard deviation, $\sqrt{\langle \delta z^2 \rangle} \sim l_p \sqrt{N_p}$, increasing with the chain length, the "quantization" is in general not observable in instantaneous configurations and emerges only in averages,

$$\bar{z}_T = \frac{1}{T} \int_t^{t+T} z(t')\, dt', \tag{81}$$

over time intervals, T, of sufficient length, where the relevant measure is the sampled number, $N_{samples} \sim T/\tau_{cor}$, of statistically *independent* configurations. The correlation time, τ_{cor}, for the fluctuating chain extension depends on the DNA dynamics in the experimental setup. A simple blob picture[42] would suggest that $\tau_{cor} \sim \phi^{-4}$ is a rapidly decreasing function of the applied force. In particular,

$$p(\bar{z}_T) = \sqrt{\frac{N_{samples}}{2\pi\langle \delta z^2 \rangle}} \exp\left(-\frac{(\bar{z}_T - \langle z \rangle_n)^2}{2\langle \delta z^2 \rangle / N_{samples}} \right). \tag{82}$$

Figure 10 illustrates the influence of the chain length, N_p, of the applied stretching force, ϕ, and of $N_{samples}$ on the distribution of (time-averaged) chain elongations for an ensemble composed of equal numbers of chains with $n-1 = 0, \ldots, 3$ nicks. There is obviously little point in exploring the effect of nicks in the weak stretching limit (left column of Fig. 10). While averaging over more and more statistically independent configurations sharpens the distributions around the mean, the peak does not split into separate peaks for molecules with different numbers of nicks. This is easy to understand. First, $\delta_\zeta(\phi)$ [and hence the distance between the quantized mean positions, Eq. (74)] vanish in this limit [Figs. 13(c), 6(c), and 9(c)]. Second, the chain fluctuations, Eq. (79), are largest because the effective spring constant for longitudinal fluctuations is a monotonously increasing function of the applied force. The signal-to-noise ratio is better in the strong stretching limit (right column of Fig. 10), but experiments might be challenging, since the *absolute* differences between the quantized elongations vanish again with $\delta_\zeta(\phi)$. From an experimental point of view, the optimal regime is, thus, probably located around intermediate forces, $\phi \approx 1$, where chains are stretched to about half their full elongation (central column of Fig. 10). Comparisons between the three rows of Fig. 10 illustrate the effect of chain length on the detection of

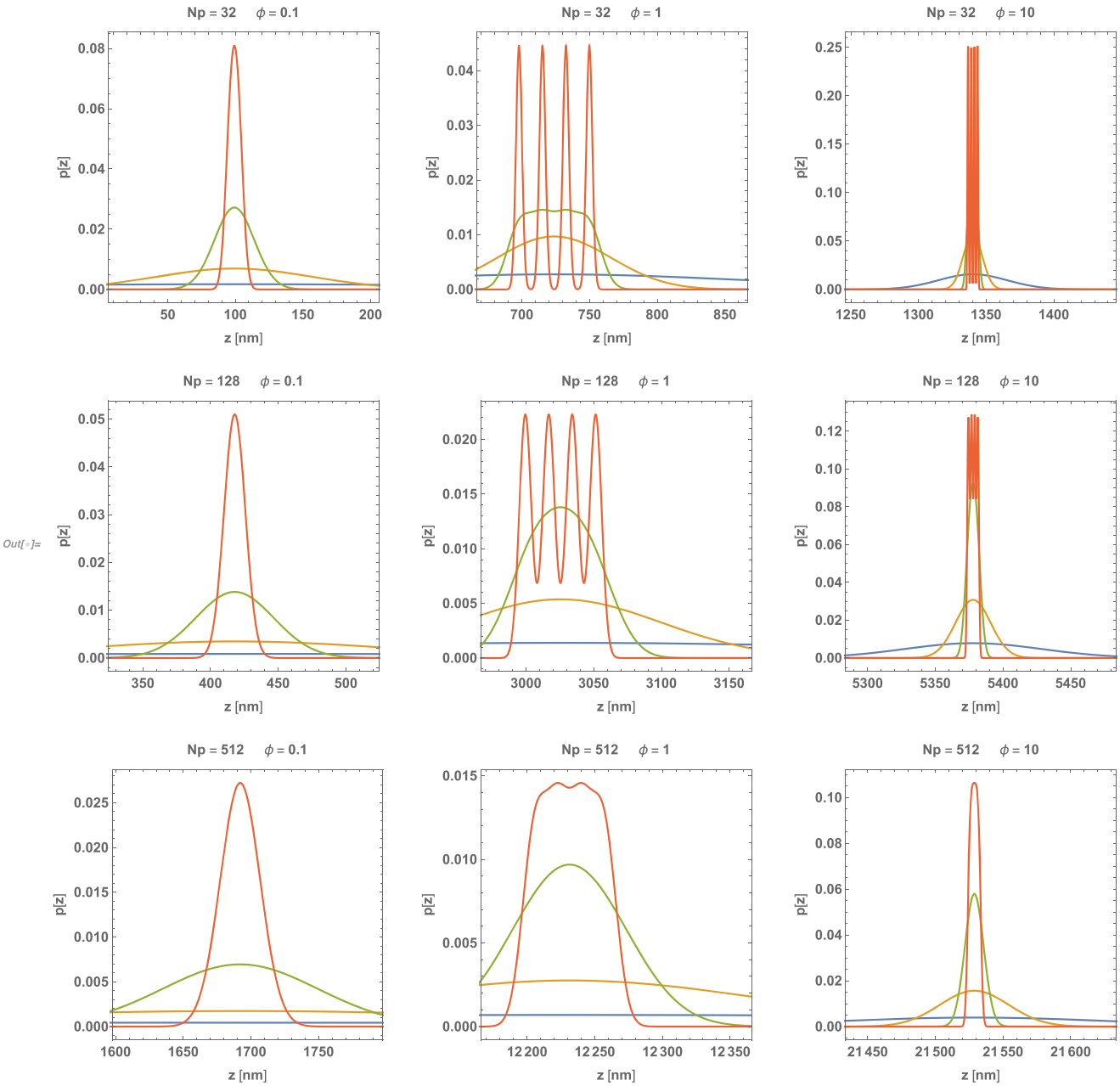

FIG. 10. Distribution of the parallel elongation for an ensemble of stretched ds-DNA molecules with $n - 1 = 0, 1, 2, 3$ nicks modeled as a corresponding sequence of freely jointed BRE-springs. The panels illustrate the effect of varying the total chain length, $N_p = 32, 128, 512$, and the applied force, $\phi = fl_p/k_BT = 0.1, 1.0, 10.0$ [for the example of ds-DNA with $l_p = 50$ at room temperature $k_BT \approx 4$ pN nm, this corresponds to ≈0.008 pN, 0.08 pN, 0.8 pN]. Blue: instantaneous elongations. Yellow, green, and red: "time averages" over $N_{samples} = 16, 256, 4096$ independent configurations. Chain elongations are reported in "nm" for the example of ds-DNA with $l_p = 50$ nm. To simplify the comparison, all panels are centered on the elongation predicted by the asymptotic elongation–force relation, $L\zeta(\phi)$, and reported $p(z)$ over z-values in intervals of an identical width of $4l_p = 200$ nm.

nicks. The effect of fluctuations decreases with N_p, if one considers the *relative* chain elongation, $\zeta = z/L$, which we have privileged throughout most of the article. However, in absolute terms, Eq. (79), the width of the fluctuations *increases* with chain length. Since the distances between the mean positions are independent of length [Eq. (74)], $N_{samples} \sim N_p$ statistically independent configurations are expected to be needed to discriminate the number of nicks in the molecule.

VI. SUMMARY AND CONCLUSIONS

The present work discusses the force–elongation and elongation–force relations of long polymer chains in single-molecule stretching experiments in the constant-force and constant-elongation ensembles. In particular, we show how to systematically derive these relations from a *given* radial end-to-end distance distribution and provide insight into the form and origin of the leading finite chain length corrections. The exactly solvable, non-trivial case of FENE-springs serves as a useful validation of our formalism and the employed numerical techniques.

In particular, we have used our formalism to explore the properties of "BTB"-springs and "BRE"-springs defined through approximate, closed analytical expressions for the end-to-end distance distribution of the WLC.[26,29] While the BTB-distribution [Eq. (59)] derives from a variational treatment, the BRE-distribution [Eq. (60)] interpolates between all relevant, exactly known limiting cases from stiff to flexible chains and from looped to fully stretched configurations. For the present application to long WLCs, it was sufficient to analyze Eq. (61). To test the quality of the BTB-approximations and BRE-approximations in the present context, we have performed Monte Carlo simulations of stretched WLCs.

The asymptotic BRE force–elongation relation [Eq. (62)] reproduces the numerical solution of Marko and Siggia's exact description[16] to within 2%. While this is probably less useful for experimental applications than the fit by Bouchiat *et al.*[20] of the exact MS relation, our formula has the merit of being the most precise among those resulting from a systematic theoretical approach to the problem.[16,19,20]

From our comparison to numerical data for the WLC, we tentatively conclude that the BRE-expressions for the finite chain length corrections in the two ensembles are of comparable quality. We argue that this precision might allow for an experimental application in the counting of "nicks" in single-molecule stretching experiments of ds-DNA because their primary effect is the reduction of the effective chain length. As details on the form of the surface anchoring can lead to corrections of similar magnitude,[43] it might be difficult to count their *absolute* number. However, the quantization of the mean elongations should allow following dynamic *changes* in the number of kinks provided they occur sufficiently slowly.

While the present work focuses on long WLCs, it might also be interesting to review the opposite limit of short WLCs with $L \lesssim l_p$ along similar lines. Figure 11 illustrates why the formalism from Sec. III has to break down for short chains, even though the BRE-distribution describes the WLC for arbitrary ratios of l_p/L and r/L. *A priori*, the limit of very short (and hence rigid) chains is described by the classical Langevin-formalism for individual or freely jointed chains.[44] Nevertheless, a quantitative analysis of the fluctuations (including a two-state model for kinking[45]) might be called for to detect transient extreme bending at these scales in single-molecule stretching experiments.[46]

With respect to the theory of WLC, we notice that the partition function $\mathcal{Z}(f)$, Eq. (39), is equivalent to the Laplace–Fourier transform of the end-to-end distribution function $Q(\vec{r})$ for which suitable sophisticate approximation schemes (such as the continued-fraction expansion of Ref. 47 or the Mathieu function expansion for $2d$ WLCs

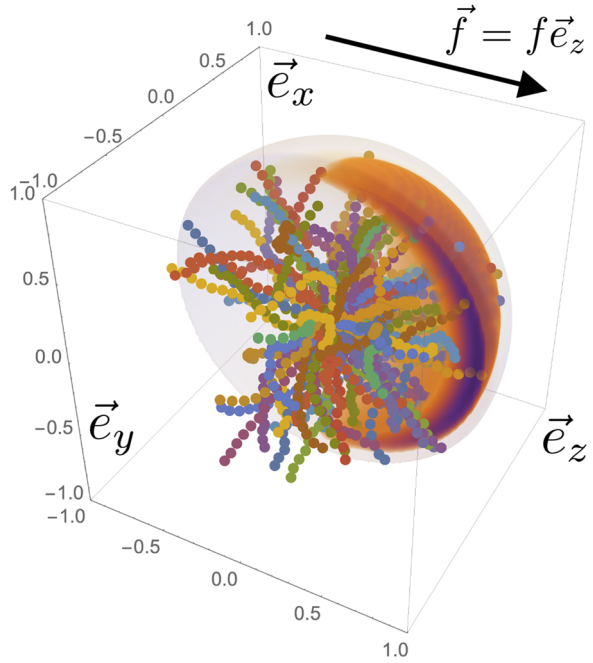

FIG. 11. Simulated chain conformations and chain-end density distributions predicted by the BRE-distribution from Ref. 26 for chain length $N_p = 1$ (=single ds-DNA filament of 150 bp) at the applied force $f = k_BT/l_p$ (=0.1 pN for ds-DNA). Notation and symbols are as in Fig. 2.

of Ref. 48) have been proposed. In future work, it might be interesting to explore if these formalisms provide an alternative access to the asymptotic WLC force–elongation relation and to the finite-size corrections in the different ensembles.

Finally, we speculate that the convenient mathematical properties of the FENE-model and our present results might be useful for the analysis[17] of analogous experiments on protein and polysaccharide stretching, where the use of the WLC model is less pertinent than for ds-DNA.

ACKNOWLEDGMENTS

R.E. gratefully acknowledges discussions with G. S. Grest in a different context, which, nevertheless, triggered the present investigation. Our work was supported by a STSM Grant from COST Action under Grant No. CA17139 (EUTOPIA). Furthermore, we benefitted from stimulating discussions with D. Thirumalai during the "Biological Physics of Chromosomes" program organized at the Kavli Institute for Theoretical Physics (Santa Barbara, USA) supported by the NSF under Grant No. PHY-1748958, the NIH under Grant No. R25GM067110, and the Gordon and Betty Moore Foundation under Grant No. 2919.02. Finally, we acknowledge the computer facilities of FLMSN, notably of Pôle Scientifique de Modélisation Numérique (PSMN) and Centre Blaise Pascal (CBP)

at Ecole Normale Supérieure de Lyon where simulations were performed.

APPENDIX A: MONTE CARLO SIMULATIONS AND DATA ANALYSIS

In the context of Sec. III, it was natural to first explore the constant-elongation ensemble and, in the second step, to use the obtained results as a basis for deriving the behavior in the constant-force ensemble. For our numerical work, it turns out to be easier to proceed in the opposite direction. Section A 1 outlines (almost trivial) Monte Carlo simulations of stretched FENE-springs, BTB-springs, and BRE-springs, while Sec. A 2 briefly describes high-precision Monte Carlo (MC) computer simulations of a standard[26] numerical model of the corresponding WLC. In the second step, discussed in Sec. A 3, we calculate the *average* force at given *constant* elongation by analyzing the distribution function of spatial elongations in the constant-force ensemble.

1. Elongation–force relations from Monte Carlo simulations of stretched FENE-springs, BTB-springs, and BRE-springs

Given an analytic expression for the end-to-end distance distribution, $Q(r)$, the expectation value

$$\langle z(f)\rangle = \frac{\int d\vec{r}\, Q(r)\, z \exp\left(\frac{f z}{k_B T}\right)}{\int d\vec{r}\, Q(r) \exp\left(\frac{f z}{k_B T}\right)} \tag{A1}$$

is straightforward to sample using Metropolis Monte Carlo simulations.[49] Starting from an arbitrary initial elongation, $\vec{r}$, with $|\vec{r}| \le L$, random changes in the end-to-end vector are accepted with a probability

$$\mathrm{acc}\left(\vec{r} \to \vec{r}\,'\right) = \min\left(1, \frac{Q(|\vec{r}\,'|) \exp\left(\frac{f z'}{k_B T}\right)}{Q(|\vec{r}|) \exp\left(\frac{f z}{k_B T}\right)}\right), \tag{A2}$$

where $Q(|\vec{r}| > L) \equiv 0$.

Specifically, a single Monte Carlo step consists of the following. At each given force f, we extract two uniformly distributed random numbers $|\vec{r}\,'|/L \in [0,1]$ and $z'/L \in [-1,+1]$ and move to this new position according to the probability equation (A2). New positions are sampled each 10^3 Monte Carlo steps, for a total of 10^6 sampled positions per each force f, which corresponds to the statistics used for the WLC model (see Sec. A 2).

Results for FENE-springs [$Q(\vec{r})$, Eq. (58)], BTB-springs [$Q(\vec{r})$, Eq. (59)], and BRE-springs [$Q(\vec{r})$, Eq. (60)] modeling polymer chains made of $N_p = 4, 8, 16, 32$ persistence lengths are shown in Figs. 13, 15, and 6 (symbols) and are in excellent agreement with theoretical results (lines, see Appendixes C and D and Sec. IV D for details). Reported error bars are calculated as the standard deviations of the corresponding means.

2. Elongation–force relations from Monte Carlo simulations of moderately stretched WLCs

Results for WLCs of numerical quality comparable to the ones established for FENE-springs, BTB-springs, and BRE-springs can be obtained from high-precision Monte Carlo (MC) computer simulations of the following standard[26] numerical model.

We have considered linear polymer chains made of $N_b \equiv L/b = 512$ rigid bonds, where b is the bond length. The energy of the chain is expressed by the Hamiltonian

$$\mathcal{H} = \mathcal{H}_{\mathrm{stiff}} + \mathcal{H}_{\mathrm{force}}. \tag{A3}$$

$\mathcal{H}_{\mathrm{stiff}}$ models the stiffness of the fiber and is given by

$$\mathcal{H}_{\mathrm{stiff}} = -k_{\mathrm{stiff}} \sum_{i=1}^{N_b-1} \hat{t}_i \cdot \hat{t}_{i+1}, \tag{A4}$$

where $\hat{t}_i = \frac{\vec{r}_i - \vec{r}_{i-1}}{b}$ is the i-th unit bond vector and $\vec{r}_i$ ($i = 0, \ldots, N$) is the spatial position of the i-th bead. The stiffness parameter k_{stiff} determines the persistence length l_p of the polymer chain. In fact, the bond–bond correlation function for $\mathcal{H}_{\mathrm{force}} = 0$ is given by

$$\langle \hat{t}_{i+j} \cdot \hat{t}_i \rangle = \exp(-b|j|/l_p), \tag{A5}$$

with

$$\frac{l_p}{b} = -\frac{1}{\log\left(\coth\left(\frac{k_{\mathrm{stiff}}}{k_B T}\right) - \frac{k_B T}{k_{\mathrm{stiff}}}\right)}. \tag{A6}$$

It is easy to see that $\lim_{k_{\mathrm{stiff}} \to \infty} l_p/b \simeq k_{\mathrm{stiff}}/k_B T$. The force term

$$\mathcal{H}_{\mathrm{force}} = -\vec{f} \cdot (\vec{r}_{N_b} - \vec{r}_0) = -f(z_{N_b} - z_0) \tag{A7}$$

stretches the chain along the z-direction.

MC moves are based on the pivot algorithm.[50,51] A monomer i between 0 and $N_b - 1$ is randomly selected, and the portion of the chain comprising monomers $i, \ldots, N_b$ is rotated by an angle randomly picked in $[0, 2\pi]$ around an axis centered on the monomer i and randomly oriented on the unit sphere. The move changes the set $\{\vec{r}\}$ of chain coordinates into $\{\vec{r}\,'\}$ and is then accepted according to the probability

$$\mathrm{acc}\left(\vec{r} \to \vec{r}\,'\right) = \min\left(1, \exp\left(-\frac{\mathcal{H}(\{\vec{r}\,'\}) - \mathcal{H}(\{\vec{r}\})}{k_B T}\right)\right). \tag{A8}$$

Single chain conformations are sampled at each $10^3 N_b$ MC moves, for a total of 10^6 conformations per each force f.

As in the case of FENE-springs, BTB-springs, and BRE-springs (Sec. A 1), we have simulated chains of a total length of $N_p = L/l_p = 32, 16, 8, 4$ persistence lengths, in order to be able to extrapolate to the asymptotic limit and to explore finite chain-length effects. While ideally we would like to study the WLC in the continuum limit with $b \to 0$, we have obtained data for discrete bond lengths of $b/l_p = 1/16, 1/32, 1/64, 1/128 \ll 1$ or $N_b = 16, 32, 64, 128N_p$. In particular, the choice of a bond length limits the range of forces, $f \ll k_BT/b$, which we can explore without encountering discretization effects. In practical terms, we have sampled f in the interval $[f_{\max}/1024, f_{\max}]$ in log-steps of 2 with $f_{\max} = \frac{1}{16}\frac{k_BT}{b}$. Corresponding results shown in Fig. 9 (symbols) are in good agreement with theoretical results for BRE-springs (lines).

3. Force–elongation relations from data obtained in the constant-force ensemble

The elongation–force relation in the constant-force ensemble is given by the sampled average chain elongations, $\langle z(f)\rangle$. In addition, one can sample corresponding histograms, $p_f(z)$. Following the discussion in Sec. III B, these histograms are peaked at an elongation $z^*(f)$, which is, in general, different from $\langle z(f)\rangle$. By correcting for the sampling bias due to the applied force, these histograms also provide a local estimate of the partition function, $\mathcal{Z}(z)$, in the constant elongation ensemble,

$$\mathcal{Z}(z) \propto p_f(z)\, \exp\left(-\frac{f\,z}{k_BT}\right). \tag{A9}$$

This estimate will be efficiently sampled in the vicinity of $z^*(f)$, and multiple such local estimates could be tiled to estimate all of $\mathcal{Z}(z)$. Using Eq. (13), we can directly estimate the force–elongation relation over the sampled z-range as

$$\langle f(z)\rangle = f - k_BT\frac{p_f'(z)}{p_f(z)}. \tag{A10}$$

In particular,

$$\langle f(z^*)\rangle = f \tag{A11}$$

at the peak of the sampled distribution, where the statistical quality of the results is highest.

The average location of the peak as a function of f is determined as follows. At each applied force f, we computed ten independent distributions $p_f(z)$ from the 10^6 sampled elongations (Sec. A 1). Then, the position of the peak of each distribution is estimated by the best fit of $\log p_f(z)$ to the function $a - \frac{k_2}{2}(z-z^*)^2 - \mathrm{sign}(z-z^*)\log(1+\frac{k_3}{6}|z-z^*|^3)$, i.e., the Gaussian function corrected for "skewness" with fit parameters a, k_2, k_3, and z^*. We have found that the position of the maximum is accurately captured by limiting the fit to ±1 standard deviation around the corresponding mean and estimating $p_f(z)$ from the histogram obtained by partitioning this interval into 40 equally spaced bins.

The symbols in Figs. 12, 14, 5, and 8 represent $\langle z^*(f)\rangle$ for FENE-springs, BTB-springs, BRE-springs, and WLC, respectively. Reported error bars indicate the standard error of the estimated means.

We take the excellent agreement of our numerical results for FENE-springs with the exact solution of the model (symbols vs lines in Figs. 12 and 13) as proof of the reliability of our method for converting between the two ensembles. The numerical data for BTB-springs and BRE-springs serve to validate our analysis of their asymptotic behavior (Figs. 5 and 6) and can be directly compared to results for BTB-springs and WLC of finite length (Figs. 8 and 9).

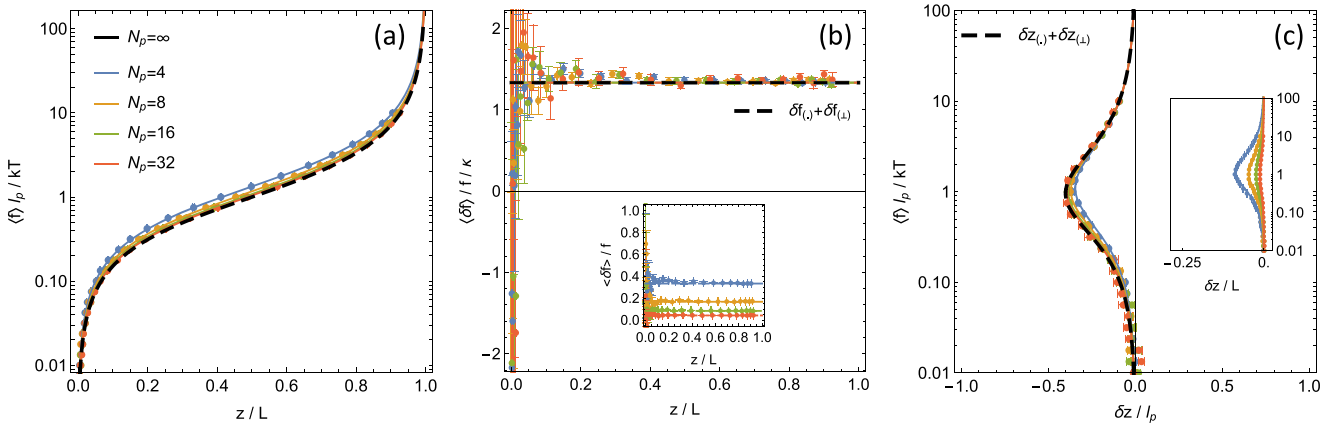

FIG. 12. FENE-springs in the constant-elongation ensemble: (a) force–elongation relations, (b) finite-size corrections to the force–elongation relation, and (c) finite-size corrections to the inverted force–elongation relation. Symbols represent the most likely elongation of FENE-springs in MC simulations in the constant-*force* ensemble (see Sec. A 3). Label notation is as in Fig. 5.

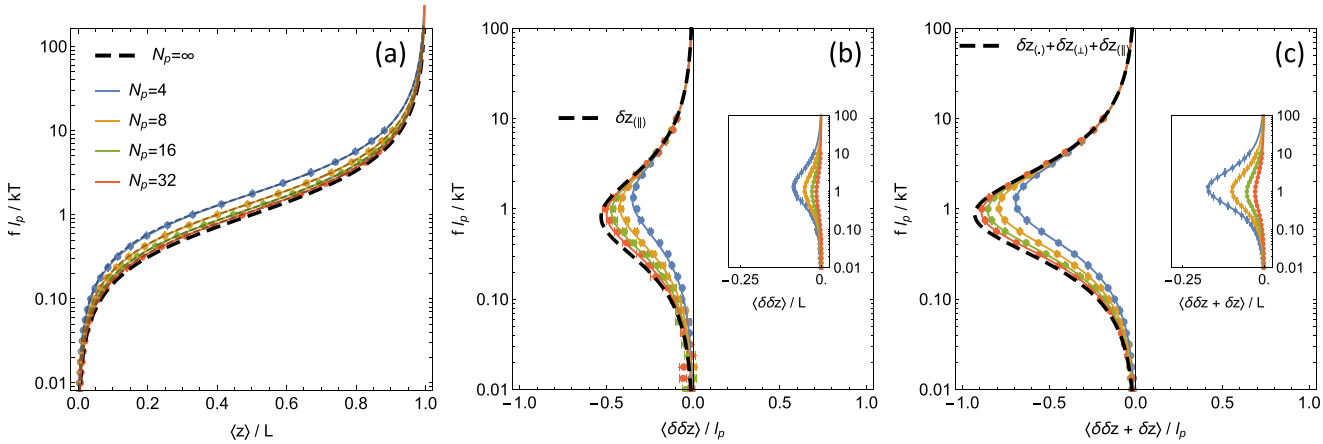

FIG. 13. FENE-springs in the constant-force ensemble: (a) elongation–force relations, (b) finite-size corrections to the inverted force–elongation relations for chains of the same length, and (c) finite-size corrections to the asymptotic elongation–force relation. Dashed colored lines in panel (a) indicate the result of the Olver expansion, Eq. (C6), while solid lines indicate the exact elongation–force relation, Eq. (C4). Symbols represent the average elongation of FENE-springs in MC simulations in the constant-force ensemble (see Sec. A 1). Note that all results are shown with the dependent variable on the abscissa to simplify the comparison with Fig. 12. Label notation is as in Fig. 6.

APPENDIX B: STRETCHING GAUSSIAN SPRINGS

1. Exact solution

Adopting the Gaussian chain model, Eq. (57), for arbitrary distances, different spatial dimensions remain uncoupled. As a consequence, $\mathcal{Z}(z) \propto \exp\left(-\frac{3}{4}N_p\left(\frac{z}{L}\right)^2\right)$, and the exact force–elongation relation,

$$\frac{\langle f(z)\rangle}{k_BT/l_p} = \frac{3}{2}\frac{z}{L}, \tag{B1}$$

follows immediately. Similarly, with $\mathcal{Z}(f) \propto \exp\left(\frac{1}{3}N_p\left(\frac{fl_p}{k_BT}\right)^2\right)$, one obtains

$$\frac{\langle z(f)\rangle}{L} = \frac{2}{3}\frac{f}{k_BT/l_p} \tag{B2}$$

for the elongation–force relation.

2. Asymptotic behavior

As there are no finite-size corrections to the force–elongation and elongation–force relations of Gaussian chains, Eqs. (B1) and (B2), the two relations are each other's inverse.

Following the analysis in Sec. III A 2, we should be able to derive the same result from the asymptotic partition function per persistence length for chains extended to the minimal end-to-end distance, $r = z$. With

$$\mathcal{Z}_{p,(\cdot)}(z/L) \propto \exp\left(-\frac{3}{4}\left(\frac{z}{L}\right)^2\right), \tag{B3}$$

it is straightforward to see that Eq. (30) yields, indeed, the correct result,

$$\frac{f_{(\cdot)}(z/L)}{k_BT/l_p} = \frac{3}{2}\frac{z}{L}. \tag{B4}$$

3. Finite chain length corrections

Do we understand the absence of corrections? It turns out that $\mathcal{Z}_{p,(\cdot)}(z/L,\kappa) = \mathcal{Z}_{p,(\cdot)}(z/L)$ independently of chain length. As there are no finite size corrections to the dominant free energy contribution, $\mathcal{F}_{p,(\cdot)}(z/L)$, there are also no corresponding corrections, Eq. (31), to the elastic response,

$$\frac{\delta f_{(\cdot)}(z/L)}{k_BT/l_p} = 0. \tag{B5}$$

Similarly, there is neither a finite-size correction, Eq. (38), to the force–elongation curve due to transverse fluctuations,

$$\frac{\delta f_{(\perp)}(z/L)}{k_BT/l_p} = 0, \tag{B6}$$

nor a correction to the elongation–force relation, Eq. (56), due to longitudinal fluctuations,

$$\frac{\delta z_{(\|)}(z/L)}{L} = 0, \tag{B7}$$

since the asymptotic force–elongation relation, $f(z) = kz$, is harmonic.

APPENDIX C: STRETCHING FENE-SPRINGS

1. Exact solution

For FENE-springs, Eq. (58), all quantities of interest can be calculated exactly. Integrating out transverse fluctuations yields

$$\mathcal{Z}(z/L, N_p) \propto \left(1 - \left(\frac{z}{L}\right)^2\right)^{\frac{3}{4}N_p+1}. \tag{C1}$$

Figure 12(a) illustrates the resulting force–elongation relation,

$$\frac{\langle f(z)\rangle}{k_BT/l_p} = \left(\frac{3}{2} + \frac{2}{N_p}\right)\frac{\left(\frac{z}{L}\right)}{1-\left(\frac{z}{L}\right)^2}, \tag{C2}$$

for a number of chain lengths, $N_p = 1/\kappa = 4, 8, 16, 32$. As expected, the elastic response reduces to the Gaussian behavior for small elongations and diverges on approaching the limit of maximal elongation. There are discernable finite-size effects as shorter chains require a larger force to be constrained at a given relative elongation.

The partition function for the constant-force ensemble, Eq. (39), can also be calculated exactly and is given by

$$\mathcal{Z}\left(\frac{fl_p}{k_BT}, N_p\right) \propto \frac{\mathrm{I}_{\frac{3}{2}+\frac{3}{4}N_p}\left(N_p\frac{fl_p}{k_BT}\right)}{\left(N_p\frac{fl_p}{k_BT}\right)^{\frac{3}{2}+\frac{3}{4}N_p}}, \tag{C3}$$

where $\mathrm{I}_\nu(x)$ denotes the modified Bessel function of the first kind and order ν. By using Eqs. (40) and (42) and employing the identity $x\,\mathrm{I}'_\nu(x) = x\,\mathrm{I}_{\nu+1}(x) + \nu\,\mathrm{I}_\nu(x)$, the corresponding elongation–force relation takes the form

$$\frac{\langle z(f)\rangle}{L} = \frac{\mathrm{I}_{\frac{5}{2}+\frac{3}{4}N_p}\left(N_p\frac{fl_p}{k_BT}\right)}{\mathrm{I}_{\frac{3}{2}+\frac{3}{4}N_p}\left(N_p\frac{fl_p}{k_BT}\right)}. \tag{C4}$$

Equations (C3) and (C4) are difficult to interpret, since both, the order and the argument of the involved Bessel functions, depend on N_p. With $0 < z \equiv x/\nu < +\infty$, Olver's uniform asymptotic expansion,[52]

$$\begin{aligned} I_\nu(x) &\sim \frac{e^{\nu\eta(z)}}{(1+z^2)^{1/4}}, \\ \eta(z) &= (1+z^2)^{1/2} + \log\frac{z}{1+(1+z^2)^{1/2}}, \end{aligned} \tag{C5}$$

depends on their *ratio* and helps reduce the chain length dependence to a correction. Substituting in Eq. (C3), using dimensionless variables, and differentiating yield

$$\begin{aligned} \langle\zeta(\phi)\rangle = {} & \frac{\sqrt{9+36\kappa(1+\kappa)+16\phi^2}}{4\phi} \\ & - \frac{3}{4\phi}\,\frac{9(1+2\kappa)^3 + 16(1+8\kappa/3)\phi^2}{9+36\kappa(1+\kappa)+16\phi^2}. \end{aligned} \tag{C6}$$

Figure 13 shows elongation–force relations for the same chain lengths as in Fig. 12. The results are shown with the dependent variable on the abscissa to simplify the comparison with the force–elongation curves. The two sets of curves are qualitatively similar, but the finite-size effects are stronger for elongation–force relations. For chains with $N_p \geq 8$, the Olver approximation, Eq. (C6), becomes virtually indistinguishable from the exact result, Eq. (C4).

2. Asymptotic behavior

The asymptotic force–elongation relation for FENE-springs,

$$\frac{f(z/L)}{k_BT/l_p} = \frac{3}{2}\frac{\left(\frac{z}{L}\right)}{1-\left(\frac{z}{L}\right)^2}, \tag{C7}$$

can be read off straightforwardly from Eq. (C2) and is indicated in Figs. 12(a) and 13(a) as a dashed black line. In particular, with

$$\lim_{z\to L}\frac{f(z/L)}{k_BT/l_p} = \frac{3}{4}\frac{1}{1-z/L}, \tag{C8}$$

the elastic response diverges on approaching full elongation.

The same result, $f(z/L) = f_{(\cdot)}(z/L)$, also follows directly from $Q(r)$ via Eq. (30) by neglecting fluctuations in the asymptotic limit

$$\mathcal{Z}_{p,(\cdot)}(z/L) = \left(1-\left(\frac{z}{L}\right)^2\right)^{\frac{3}{4}}. \tag{C9}$$

The inverse of the asymptotic force–elongation relation,

$$\frac{z}{L} = \frac{\sqrt{9+16\left(\frac{fl_p}{k_BT}\right)^2}}{4\frac{fl_p}{k_BT}} - \frac{3}{4}\frac{k_BT}{fl_p}, \tag{C10}$$

agrees with Eq. (C6) in the $\kappa \to 0$-limit, where the Olver expansion becomes exact.

3. Finite chain length corrections to the force–elongation relation

The finite-size corrections to the force–elongation relation,

$$\frac{\delta f(z/L, N_p)}{k_BT/l_p} = \frac{2}{N_p}\frac{\left(\frac{z}{L}\right)}{1-\left(\frac{z}{L}\right)^2}, \tag{C11}$$

can again be read off straightforwardly from Eq. (C2). They turn out to be proportional to the asymptotic response and are shown for different chain lengths, N_p, in the inset of Fig. 12(b). In particular, the corrections are linear in κ with all higher order terms vanishing identically. As a consequence, they perfectly superimpose, when they are rescaled as $N_p\frac{\delta f(z/L)}{k_BT/l_p} = \frac{\delta f(z/L)}{k_BT/L}$ [Fig. 12(b)].

Following the analysis in Sec. III A 2, we can try to better understand the origin of the finite size corrections. As in the case of Gaussian chains, $\mathcal{Z}_{p,(\cdot)}(z/L,\kappa) = \mathcal{Z}_{p,(\cdot)}(z/L)$ independently of chain

length. In the absence of finite size corrections to the dominant free energy contribution, $\mathcal{F}_{p,(\cdot)}(z/L)$, there are also no corresponding corrections, Eq. (31), to the elastic response,

$$\frac{\delta f_{(\cdot)}(z/L, N_p)}{k_B T/l_p} = 0. \tag{C12}$$

However, for FENE-springs, the effective spring constant, $k_{(\perp)}$, for transverse fluctuations diverges on approaching full elongation. The corresponding finite-size correction, Eq. (38), for the force–elongation curve reads

$$\frac{\delta f_{(\perp)}(z/L, N_p)}{k_B T/l_p} = \frac{2}{N_p} \frac{\left(\frac{z}{L}\right)}{1 - \left(\frac{z}{L}\right)^2}, \tag{C13}$$

so that, indeed, $f_{(\cdot)} + \delta f_{(\cdot)} + \delta f_{(\perp)} = \langle f \rangle$ for all values of N_p.

4. Finite chain length corrections to the elongation–force relation

To first order in κ, the finite chain length corrections to the elongation–force relation [Eq. (C6)] read

$$\frac{\delta z(\phi, N_p)}{L} = -\frac{1}{N_p}\left(\frac{3}{2\phi} + \frac{8\phi}{9 + 16\phi^2} - \frac{9}{2\phi\sqrt{9 + 16\phi^2}}\right). \tag{C14}$$

Again, we can try to understand the origin of these finite size corrections following the analysis in Secs. III A and III B. In Figs. 12 and 13, we distinguish (i) the difference between the inverted force–elongation relations for chains of finite length and the asymptotic elongation force relation [Fig. 12(c)], (ii) the difference between the elongation–force relation and the inverted force–elongation relation for chains of a given length [Fig. 13(b)], and (iii) the difference between the elongation–force relations for chains of finite length and the asymptotic elongation–force relation [Fig. 13(c)], which is the sum of the first two terms. In all three cases, insets show the absolute corrections, which are largest for short chains, while the main panels show rescaled corrections, $N_p(\delta z/L) = \delta z/l_p$. All three corrections display qualitatively similar features. They are largest for chains, which are extended to about half of their maximal elongation, $z^*/L \approx 1/2$, and they vanish in the limits of small forces, $z^*/L \to 0$, and of maximal elongation, $z^*/L \to 1$.

For a quantitative analysis, consider first the finite-size corrections to the inverted force–elongation relation [Fig. 12(c)]. As expected, they converge to the sum of the first-order corrections arising from the dominant term and from transverse fluctuations, Eqs. (49) and (50), which, for FENE chains, are given by

$$\frac{\delta z_{(\cdot)}(z^*/L, N_p)}{L} = 0, \tag{C15}$$

$$\frac{\delta z_{(\perp)}(z^*/L, N_p)}{L} = -\frac{4}{3}\frac{1}{N_p}\frac{z^*}{L}\frac{1 - \left(\frac{z^*}{L}\right)^2}{1 + \left(\frac{z^*}{L}\right)^2} \tag{C16}$$

and which we have indicated as a dashed black line in Fig. 12(c). Note that there are higher order corrections to δz even though δf is linear in κ, since the asymptotic force–elongation relation is nonlinear.

Next, consider the difference between the elongation–force relation, $\langle z(f) \rangle$, and the inverse of the force–elongation relation, $\langle f(z) \rangle$ [Fig. 13(b)]. In agreement with our theoretical arguments for the effect of elongation-dependent longitudinal fluctuations, they converge to Eq. (56), which reads, for FENE chains,

$$\frac{\delta z_{(\parallel)}(z^*/L, N_p)}{L} = -\frac{2}{3}\frac{1}{N_p}\frac{z^*}{L}\left(\left(\frac{2}{1 + \left(\frac{z^*}{L}\right)^2}\right)^2 - 1\right). \tag{C17}$$

Last but not least, the total finite-size correction to the asymptotic elongation–force relation converges to the sum, $\delta z_{(\cdot)} + \delta z_{(\perp)} + \delta z_{(\parallel)}$, of the three correction terms [Fig. 13(c)]. In particular, this sum can be shown to be equal, Eq. (C14), by using the asymptotic force–elongation relation, Eq. (C7), to express the stretching force through z^*/L.

APPENDIX D: STRETCHING "BTB-SPRINGS" REPRESENTING LONG WLCS

1. Asymptotic behavior

In the asymptotic limit, the free energy per persistence length is dominated by the exponential term in Eq. (59),

$$\frac{\mathcal{F}_{p,(\cdot)}(z/L)}{k_B T} = \frac{3}{4}\frac{1}{1 - (r/L)^2}.$$

Differentiating with respect to the elongation, Eq. (30), yields

$$\frac{f_{(\cdot)}(z/L)}{k_B T/l_p} = \frac{3}{2}\frac{z/L}{\left(1 - (z/L)^2\right)^2} \tag{D1}$$

for the asymptotic force–elongation relation of BTB-springs [shown as a dashed black line in Figs. 14(a) and 15(a)]. BTB-springs display the same (Gaussian) small elongation behavior as FENE-springs, but their elastic response diverges more quickly on approaching full elongation,

$$\lim_{z \to L} \frac{f_{(\cdot)}(z/L)}{k_B T/l_p} = \frac{3}{8}\frac{1}{(1 - z/L)^2}. \tag{D2}$$

Note that the limiting behavior perfectly agrees with the result of the corresponding direct variational calculation for stretched WLCs.[31] The closed expression, Eq. (D1), appears to be a new result.

The asymptotic elongation–force curve, $z_{(\cdot)}(f)$, can be expressed in closed form as a root of a third order polynomial. We, nevertheless, show results in the constant-force ensemble as parametric plots of the type $f(z^*)$ vs $z(f(z^*))$ discussed in Sec. III B.

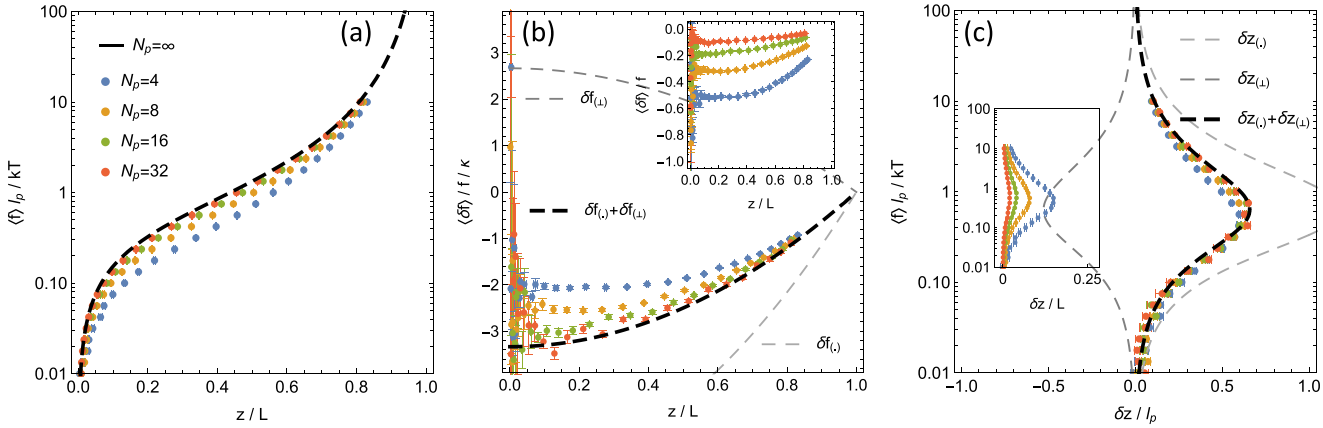

FIG. 14. BTB-springs in the constant-elongation ensemble: (a) force–elongation relations, (b) finite-size corrections to the force–elongation relation, and (c) finite-size corrections to the inverted force–elongation relation. Symbols represent the most likely elongation of BTB-springs in MC simulations in the constant-*force* ensemble (see Sec. A 3). Label notation is as in Fig. 5.

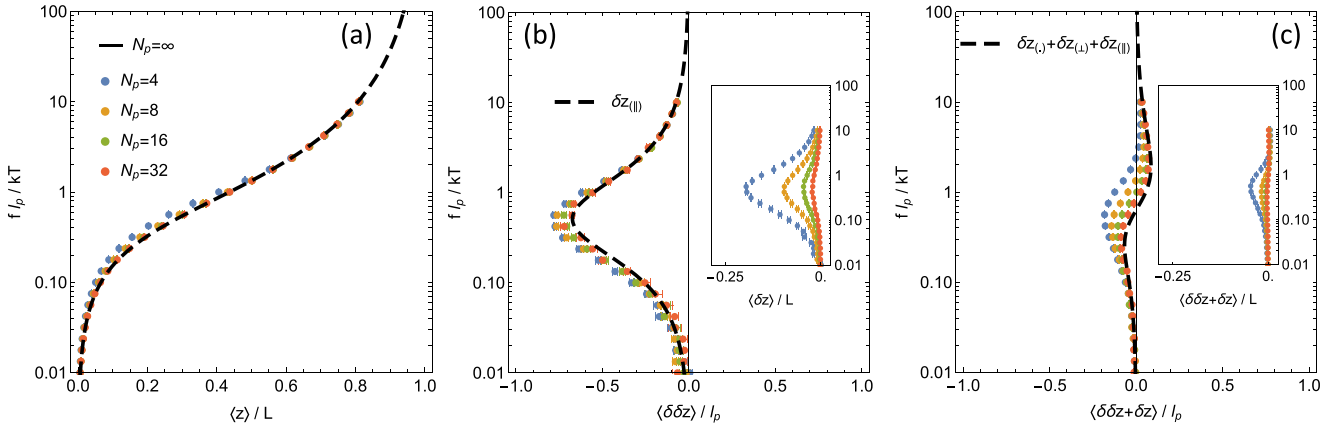

FIG. 15. BTB-springs in the constant-force ensemble: (a) elongation–force relations, (b) finite-size corrections to the inverted force–elongation relations for chains of the same length, and (c) finite-size corrections to the asymptotic elongation–force relation. Symbols represent the average elongation of BTB-springs in MC simulations in the constant-force ensemble (see Sec. A 1). Note that all results are shown with the dependent variable on the abscissa to simplify the comparison with Fig. 14. Label notation is as in Fig. 6.

2. Finite chain length corrections to the force–elongation relation

In contrast to FENE-springs, the relative finite chain length corrections to the force–elongation relation of BTB-springs are elongation dependent [panels (a) and (b) in Figs. 12 and 14]. While they vanish close to full elongation, they are more than twice as strong for moderate elongations. In particular, they are of opposite sign.

For BTB-springs, the finite-size correction, Eq. (38), due to transverse fluctuations,

$$\frac{\delta f_{(\perp)}(z/L,\kappa)}{k_BT/l_p} = 4\kappa\frac{z/L}{1-(z/L)^2}, \tag{D3}$$

has the exact same functional form as Eq. (C13) for FENE-springs but is twice as strong. In particular, Eqs. (D3) and (C13) have the same sign, since they result from the suppression of transverse fluctuations with increasing elongation.

The difference in behavior is due to the presence of finite-size corrections to the dominant free energy contribution, $\mathcal{F}_{p,(\cdot)}(z/L,\kappa)$, from aligned chains with the minimal elongation, $r = z$. As there is no explicit chain length dependence of the subdominant prefactor in Eq. (59), there are no higher order corrections to $\delta\mathcal{F}_{p,(\cdot)}(z/L,\kappa)$ beyond the linear term,

$$\frac{\delta\mathcal{F}_{p,(\cdot)}(z/L,\kappa)}{k_BT} = \frac{9}{2}\kappa\log\left(1-(z/L)^2\right).$$

Again, the corresponding correction, Eq. (31), for BTB-springs,

$$\frac{\delta f_{(\cdot)}(z/L,\kappa)}{k_BT/l_p} = -9\kappa\frac{z/L}{1-(z/L)^2}, \tag{D4}$$

has a FENE-like functional form. However, the sign is opposite because the diverging subdominant factor of $\left(1-\left(\frac{r}{L}\right)^2\right)^{-9/2}$ in Eq. (59) *reduces* the drop in $Q(r)$ on approaching full elongation. A comparison of the prefactors with Eq. (D3) shows that this latter effect is larger and, hence, the overall correction of opposite sign compared to FENE-springs. Our numerical results for BTB-springs are in excellent agreement with the results of this analysis [Fig. 14(b)].

3. Finite chain length corrections to the elongation–force relation

Following the discussions in Secs. III A and III B, the finite chain length corrections to the asymptotic force–elongation relation also cause first-order corrections to its inverse. For BTB-springs, Eqs. (49) and (50) read

$$\frac{\delta z_{(\cdot)}(z^*/L,\kappa)}{L} = +6\kappa\frac{(z^*/L)\left(1-(z^*/L)^2\right)^2}{1+3(z^*/L)^2}, \tag{D5}$$

$$\frac{\delta z_{(\perp)}(z^*/L,\kappa)}{L} = -\frac{8}{3}\kappa\frac{(z^*/L)\left(1-(z^*/L)^2\right)^2}{1+3(z^*/L)^2}. \tag{D6}$$

The two functions and their sum are shown in Fig. 14(c). Like for FENE-springs, the corrections are strongest around $z/L \approx 1/2$ and $fl_p/k_BT \approx 1$. However, the total correction has the opposite sign, and its magnitude is about 50% larger. Once more, the numerical results for BTB-springs are in excellent agreement with our analysis results.

In addition, we expect a correction due to the elongation-dependence relations. For BTB-springs, Eq. (56) reads

$$\frac{\delta z_{(\parallel)}(z^*/L,N_p)}{L} = -4\kappa\frac{\left((z^*/L)+(z^*/L)^3\right)\left(1-(z^*/L)^2\right)^2}{\left(1+3(z^*/L)^2\right)^2}. \tag{D7}$$

The correction is qualitatively similar but stronger than that for FENE-springs [panel (b) in Figs. 13 and 15]. Again, our numerical results converge to the theoretical prediction.

The total finite chain length corrections to the elongation relation of BTB-springs are shown in Fig. 15(c). Curiously, the theoretically predicted first order correction, $\delta z_{(\cdot)} + \delta z_{(\perp)} + \delta z_{(\parallel)}$, for BTB-springs almost cancels each other. Once more, the results of our simulations for BTB-springs representing WLCs with a length of $N_p = 4, \ldots, 32$ persistence lengths converge to the theoretically predicted first order correction.

DATA AVAILABILITY

The data that support the findings of this study are available from the corresponding author upon reasonable request.

REFERENCES

[1] O. Kratky and G. Porod, Recl. Trav. Chim. Pays-Bas **68**, 1106 (1949).
[2] F. Gittes, B. Mickey, J. Nettleton, and J. Howard, J. Cell Biol. **120**, 923 (1993).
[3] D. C. Morse, Phys. Rev. E **58**, R1237 (1998).
[4] B. Hinner, M. Tempel, E. Sackmann, K. Kroy, and E. Frey, Phys. Rev. Lett. **81**, 2614 (1998).
[5] R. Everaers, F. Jülicher, A. Ajdari, and A. C. Maggs, Phys. Rev. Lett. **82**, 3717 (1999).
[6] M. Pasquali, V. Shankar, and D. C. Morse, Phys. Rev. E **64**, 020802 (2001).
[7] J. Wilhelm and E. Frey, Phys. Rev. Lett. **91**, 108103 (2003).
[8] F. Pampaloni, G. Lattanzi, A. Jonáš, T. Surrey, E. Frey, and E.-L. Florin, Proc. Natl. Acad. Sci. U. S. A. **103**, 10248 (2006).
[9] C. Heussinger, B. Schaefer, and E. Frey, Phys. Rev. E **76**, 031906 (2007).
[10] J. R. Blundell and E. M. Terentjev, Macromolecules **42**, 5388 (2009).
[11] C. Heussinger, F. Schüller, and E. Frey, Phys. Rev. E **81**, 021904 (2010).
[12] Q. Wen and P. A. Janmey, Curr. Opin. Solid State Mater. Sci. **15**, 177 (2011).
[13] T. A. Hunt, S. Mogurampelly, G. Ciccotti, C. Pierleoni, and J.-P. Ryckaert, Polymers **8**, 343 (2016).
[14] F. Meng and E. Terentjev, Polymers **9**, 52 (2017).
[15] C. Bustamante, J. Marko, E. Siggia, and S. Smith, Science **265**, 1599 (1994).
[16] J. F. Marko and E. D. Siggia, Macromolecules **28**, 8759 (1995).
[17] M. Rief, J. M. Fernandez, and H. E. Gaub, Phys. Rev. Lett. **81**, 4764 (1998).
[18] S. Smith, L. Finzi, and C. Bustamante, Science **258**, 1122 (1992).
[19] A. Vologodskii, Macromolecules **27**, 5623 (1994).
[20] C. Bouchiat, M. D. Wang, J.-F. Allemand, T. Strick, S. M. Block, and V. Croquette, Biophys. J. **76**, 409 (1999).
[21] T. R. Strick, M.-N. Dessinges, G. Charvin, N. H. Dekker, J.-F. Allemand, D. Bensimon, and V. Croquette, Rep. Prog. Phys. **66**, 1 (2002).
[22] J. R. Moffitt, Y. R. Chemla, S. B. Smith, and C. Bustamante, Annu. Rev. Biochem. **77**, 205 (2008).
[23] M. Rief, M. Gautel, F. Oesterhelt, J. M. Fernandez, and H. E. Gaub, Science **276**, 1109 (1997).
[24] M. Rief, F. Oesterhelt, B. Heymann, and H. Gaub, Science **275**, 1295 (1997).
[25] M. Doi and S. F. Edwards, *The Theory of Polymer Dynamics* (Oxford University Press, New York, 1986).
[26] N. B. Becker, A. Rosa, and R. Everaers, Eur. Phys. J. E **32**, 53 (2010).
[27] M. D. Wang, H. Yin, R. Landick, J. Gelles, and S. M. Block, Biophys. J. **72**, 1335 (1997).
[28] H. Clausen-Schaumann, M. Rief, C. Tolksdorf, and H. E. Gaub, Biophys. J. **78**, 1997 (2000).
[29] J. K. Bhattacharjee, D. Thirumalai, and J. D. Bryngelson, arXiv:cond-mat/9709345 (1997).
[30] B. Y. Ha and D. Thirumalai, J. Chem. Phys. **103**, 9408 (1995).
[31] B.-Y. Ha and D. Thirumalai, J. Chem. Phys. **106**, 4243 (1997).
[32] K. Nagai, Polym. J. **4**, 35 (1973).
[33] M. Rief, H. Clausen-Schaumann, and H. E. Gaub, Nat. Struct. Biol. **6**, 346 (1999).
[34] R. M. Neumann, Biophys. J. **85**, 3418 (2003).
[35] M. Süzen, M. Sega, and C. Holm, Phys. Rev. E **79**, 051118 (2009).
[36] V. A. Ivanov, L. I. Klushin, and A. M. Skvortsov, Polym. Sci., Ser. A **54**, 602 (2012).
[37] T. R. Strick, J.-F. Allemand, D. Bensimon, and V. Croquette, Biophys. J. **74**, 2016 (1998).
[38] H. R. Warner, Ind. Eng. Chem. Fundam. **11**, 379 (1972).
[39] H. E. Daniels, Proc. R. Soc. Edinburgh **63**, 290 (1952).
[40] J. Wilhelm and E. Frey, Phys. Rev. Lett. **77**, 2581 (1996).

[41] F. Kilchherr, C. Wachauf, B. Pelz, M. Rief, M. Zacharias, and H. Dietz, Science **353**, aaf5508 (2016).
[42] P.-G. De Gennes, *Scaling Concepts in Polymer Physics* (Cornell University Press, Ithaca, 1979).
[43] I. M. Kulić, H. Mohrbach, V. Lobaskin, R. Thaokar, and H. Schiessel, Phys. Rev. E **72**, 041905 (2005).
[44] M. Rubinstein and R. H. Colby, *Polymer Physics* (Oxford University Press, New York, 2003).
[45] P. A. Wiggins, R. Phillips, and P. C. Nelson, Phys. Rev. E **71**, 021909 (2005).
[46] R. Vafabakhsh and T. Ha, Science **337**, 1097 (2012).
[47] S. Mehraeen, B. Sudhanshu, E. F. Koslover, and A. J. Spakowitz, Phys. Rev. E **77**, 061803 (2008).
[48] C. Kurzthaler and T. Franosch, Phys. Rev. E **95**, 052501 (2017).
[49] N. Metropolis, A. W. Rosenbluth, M. N. Rosenbluth, A. H. Teller, and E. Teller, J. Chem. Phys. **21**, 1087 (1953).
[50] A. D. Sokal, arXiv:hep-lat/9405016 (1994).
[51] A. D. Sokal, Nucl. Phys. B, Proc. Suppl. **47**, 172 (1996).
[52] D. E. Amos, Math. Comput. **28**, 239 (1974).